The morphodynamic evolution of Santorini volcanic complex

Pre-Conference Field Trip Guide of the IAG

RCG2019 – Regional Conference of Geomorphology

September 15th -18th, 2019

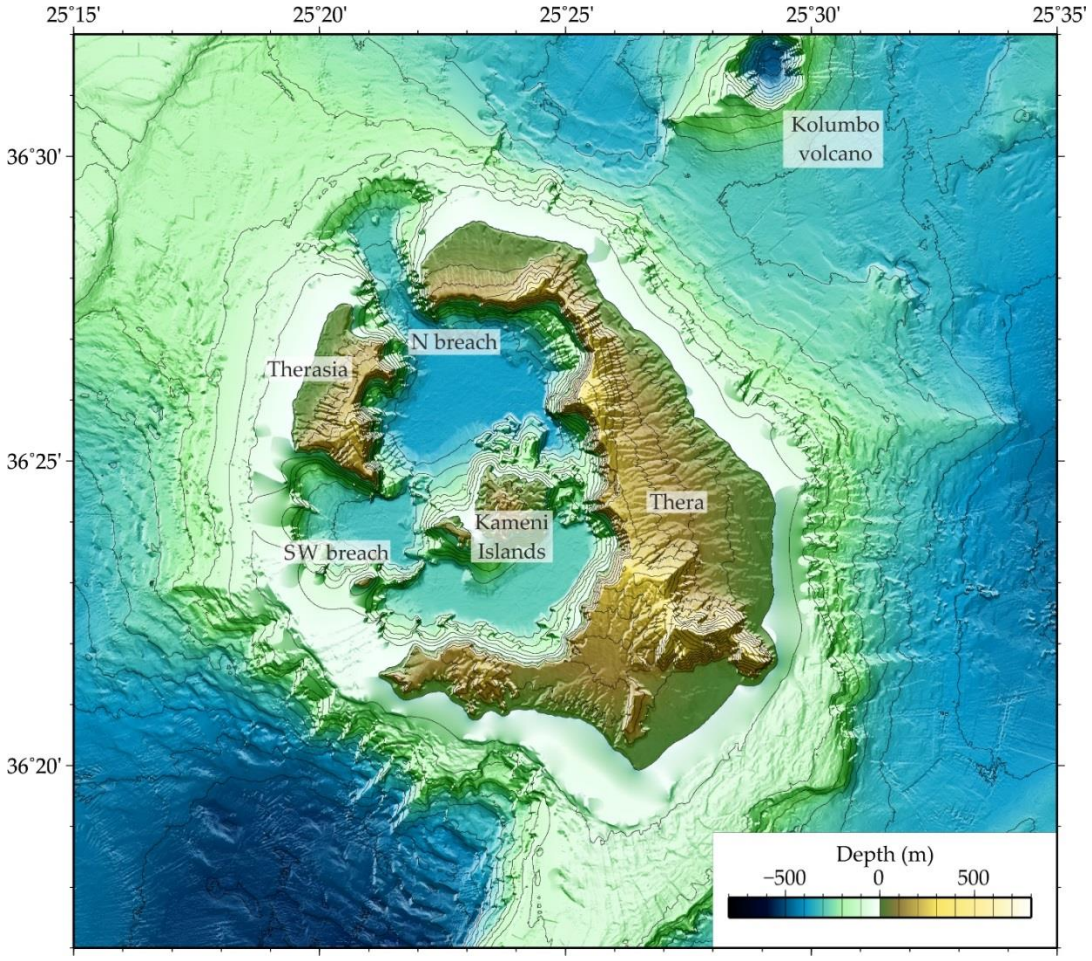

Nomikou Paraskevi, **(NKUA)** ***Vouvalidis Konstantinos,*** **(AUTH)** ***Pavlides Spyros*** **(AUTH)**

The Santorini Volcanic complex

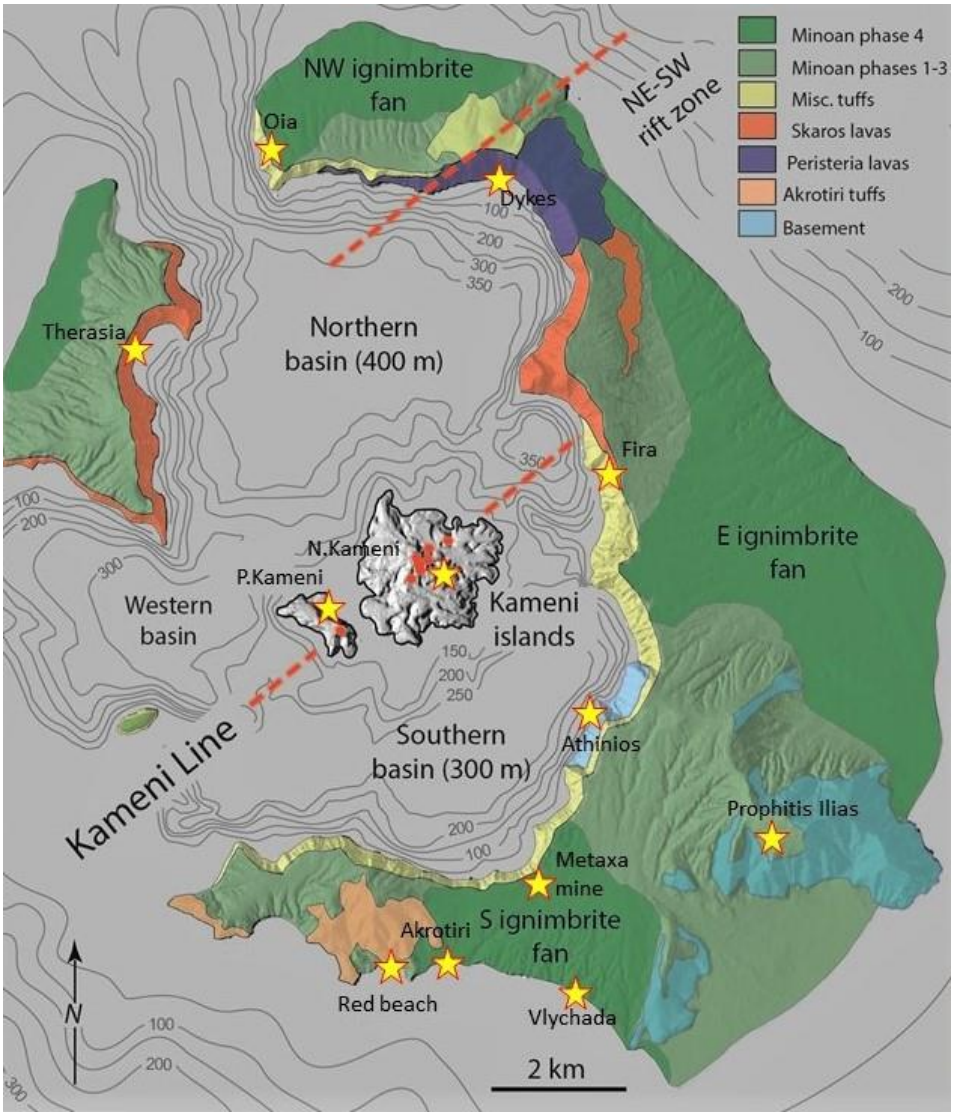

Index map showing locations of field trip stops (stars)

- ***Athinios Port (Basement lithologies) - Prophitis Ilias (Metamorphic Basement rocks)***
- ***Therasia Island (Skaros shield-Therasia dome complex-Cape Riva eruption)***
- ***Northern caldera Dyke swarm***
- ***Fira Harbor***
- ***Red Beach (Akrotiri)***
- ***Metaxa Mine (Minoan phases)***
- ***Vlychada (Minoan phases)***
- ***Akrotiri Excavations***
- ***Nea Kameni & Palaea Kameni (Eruption History – Features)***

Santorini Eruptive cycles

The history of the Santorini volcanic field is composed by 6 distinct stages. In detail, two explosive cycles which volumetrically play the most significant role on the stratigraphy of the island, contain 12 major explosive eruptions (Thera pyroclastics) and at least 3 large lava shields. The first eruptive phase (360 -172 ka) is mainly distributed in the southern Thera cliffs while the second eruptive phase (172 – 3.6 ka) is totally defining Therasia and Aspronisi and parts of the Northern and central (Fira towards the south) caldera wall (Fig. 1) (Druitt et al., 1999).

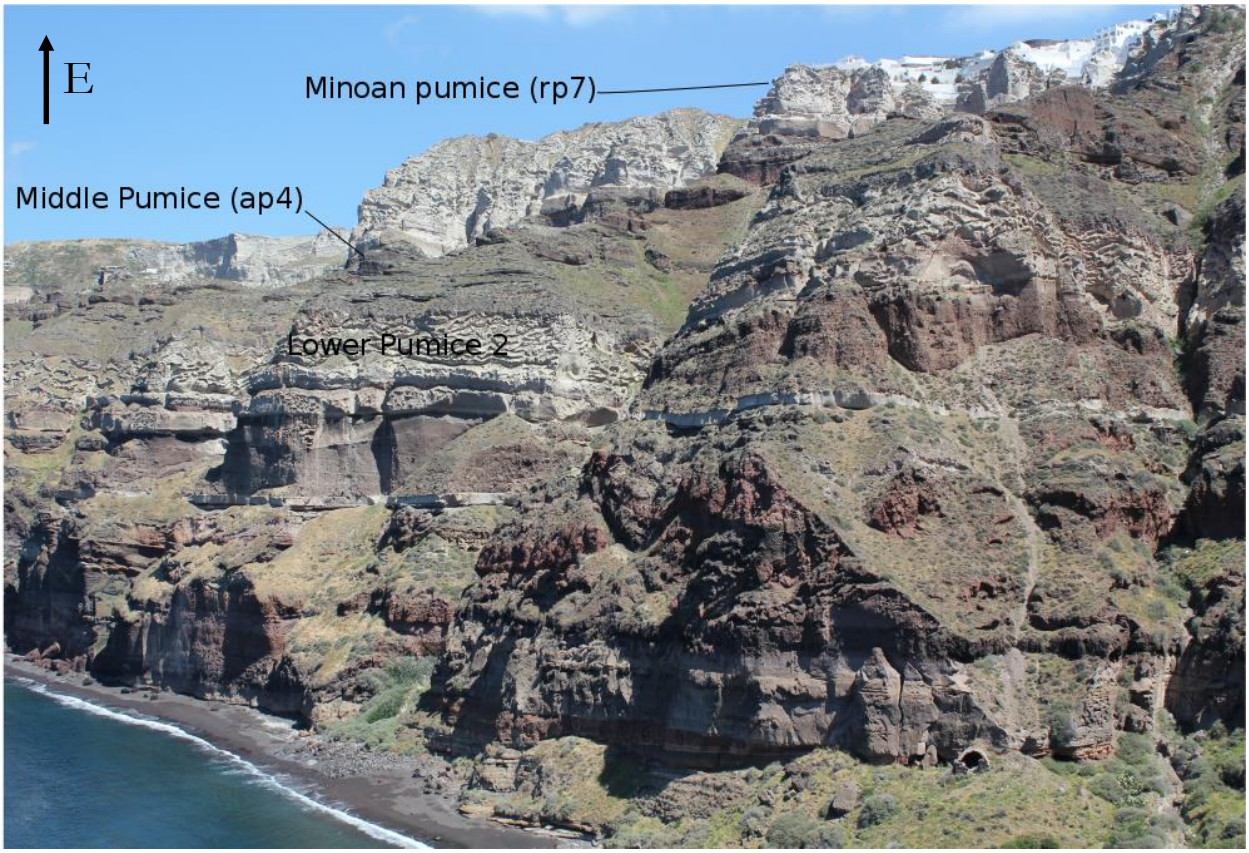

Fig.1: Panorama at Athinios Port showing the pyroclastic successions of the 2 major eruptive cycles. (Photo: A. Gudmundsson). The caldera walls are ~400m tall while they continue below the sea level up to 390m deep.

Caldera collapse events

Mechanism: Collapse caldera forms when the magma chamber cannot support the weight and associated stresses of the volcanic edifice above. Calderas never form, as far as we know, into a large empty cavity - because such cavities cannot form at many km depth. In contrary, they form as piston of rock subsides into a magma chamber while magma is, commonly, being squeezed out.

The volcanic evolution in Santorini is permeated by (at least) 4 caldera collapse events that took place during the 2 eruptive cycles since 172 ka. Each cycle began with mafic to intermediate volcanism and terminated by silicic extrusions accompanied by collapse events. The remnants of

the latter are observed on the caldera cliffs defined usually by unconformities and underlying palaeosols layers (Figs. 2, 3).

Caldera 1 (172 ka): Is located south of Thera defined by a 150 m unconformity which is covered by pyroclastic deposits.

Caldera 2 (76 ka): Is located north of Thera and is formed by the Middle tuff eruption series and covered by the Skaros lavas (67 ka).

Caldera 3 (22 ka): Is located on the present-day caldera wall at northern Thera and in Fira harbor (Minoan pumice layer- 140 m elevation)

Caldera 4 (3.6 ka): Is located mainly north of the Kameni line. At Athinios port is defined by the collapse of Minoan eruption (tuffs) which exhumed the northwest cliff and shore of the pre-volcanic basement.

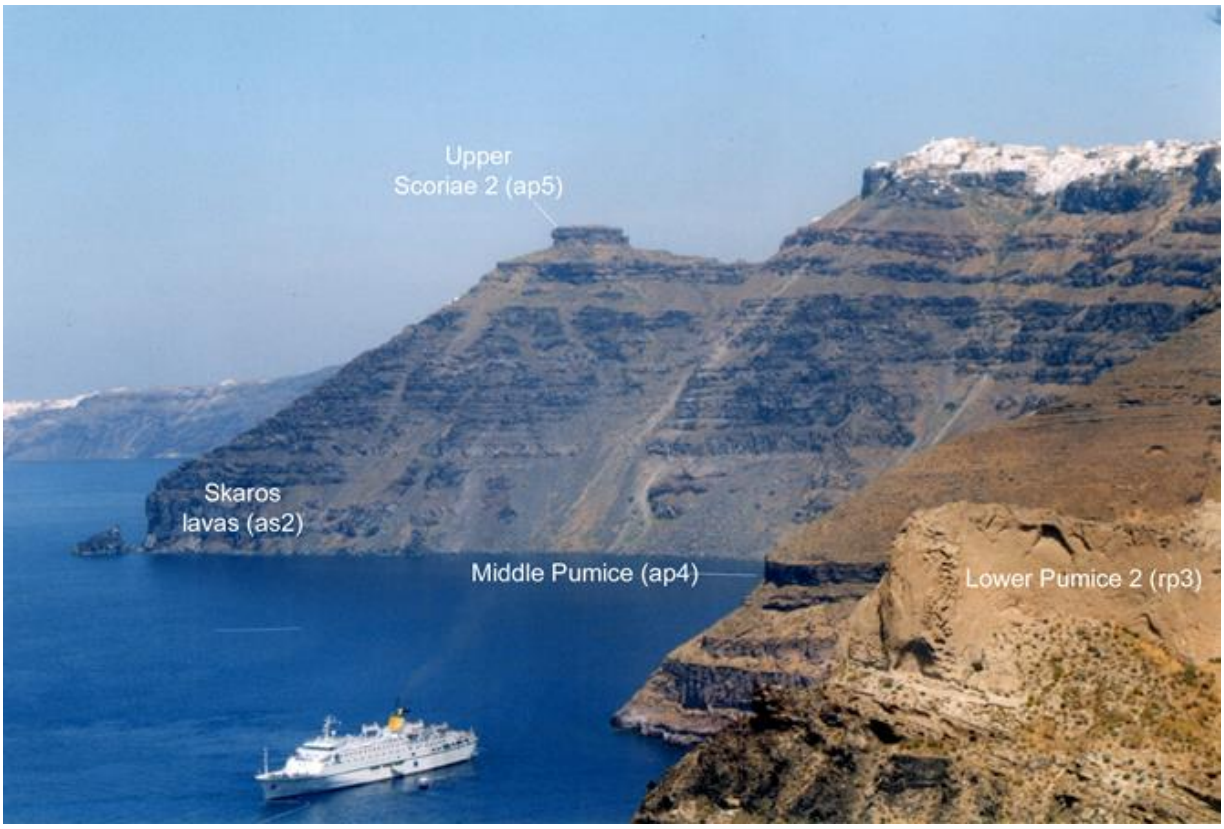

Fig.2: View of Cape Skaros (Druitt et al. 1999).

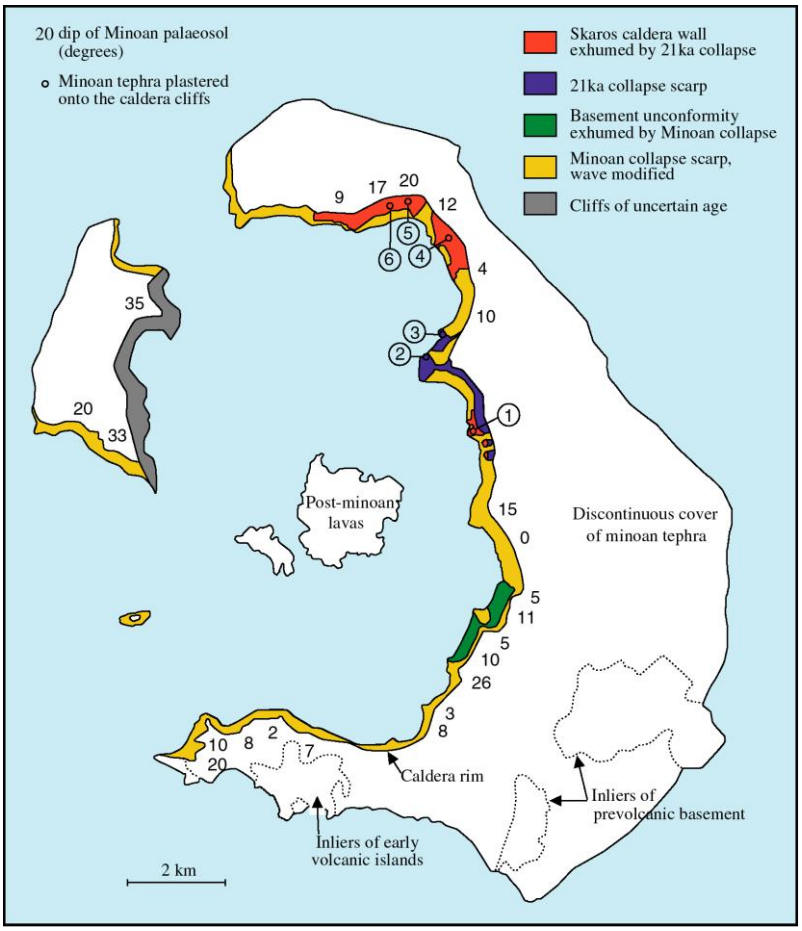

Fig.3: Geomorphological map of the caldera wall modified after Druitt and Francaviglia, 1992 showing the generations of cliff surface.

Onshore-Offshore geomorphology

The DEM of Santorini Caldera presents a relief model of Santorini caldera showing the subaerial topography and submarine bathymetry (Fig. 4). The caldera walls rise to over 300 m above sea level, while the maximum depth of the caldera seafloor is about 390 m below sea level. The present configuration of the caldera consists of three distinct basins that form separate depositional environments (Nomikou et al., 2013; 2014). The North Basin is the largest and the deepest (389 m) developed between the Kameni islands, Thirasia and the northern part of the Santorini caldera. It is connected by a narrow steep-sided channel with a depth of 300 m to a scallop-shaped ENE-WSW aligned feature that lies outside Santorini caldera, NW of Oia Village.

The smaller West Basin is encompassed by Aspronisi islet, Palea Kameni and Southern Thirasia with a moderate maximum depth – up to 325 m. The flanks of the basin are gentle in the western part and steepen close to Thirasia and Aspronisi. The South Basin is bounded by the Kameni islands (to the north) and the southern part of the Santorini caldera (to the south). It covers a larger area and is shallower by ~ 28 m than the western basin. The seafloor morphology suggests that the southern basin has been separated from the western and northern basins by the development of a series of subaerial and submarine volcanic domes, aligned in a NE-SW

direction. Apart from the subaerial Kameni islands, the most well-known submarine extrusion is the reef close to Fira Port, which has grown from 300 m b.s.l. up to 40 m b.s.l.

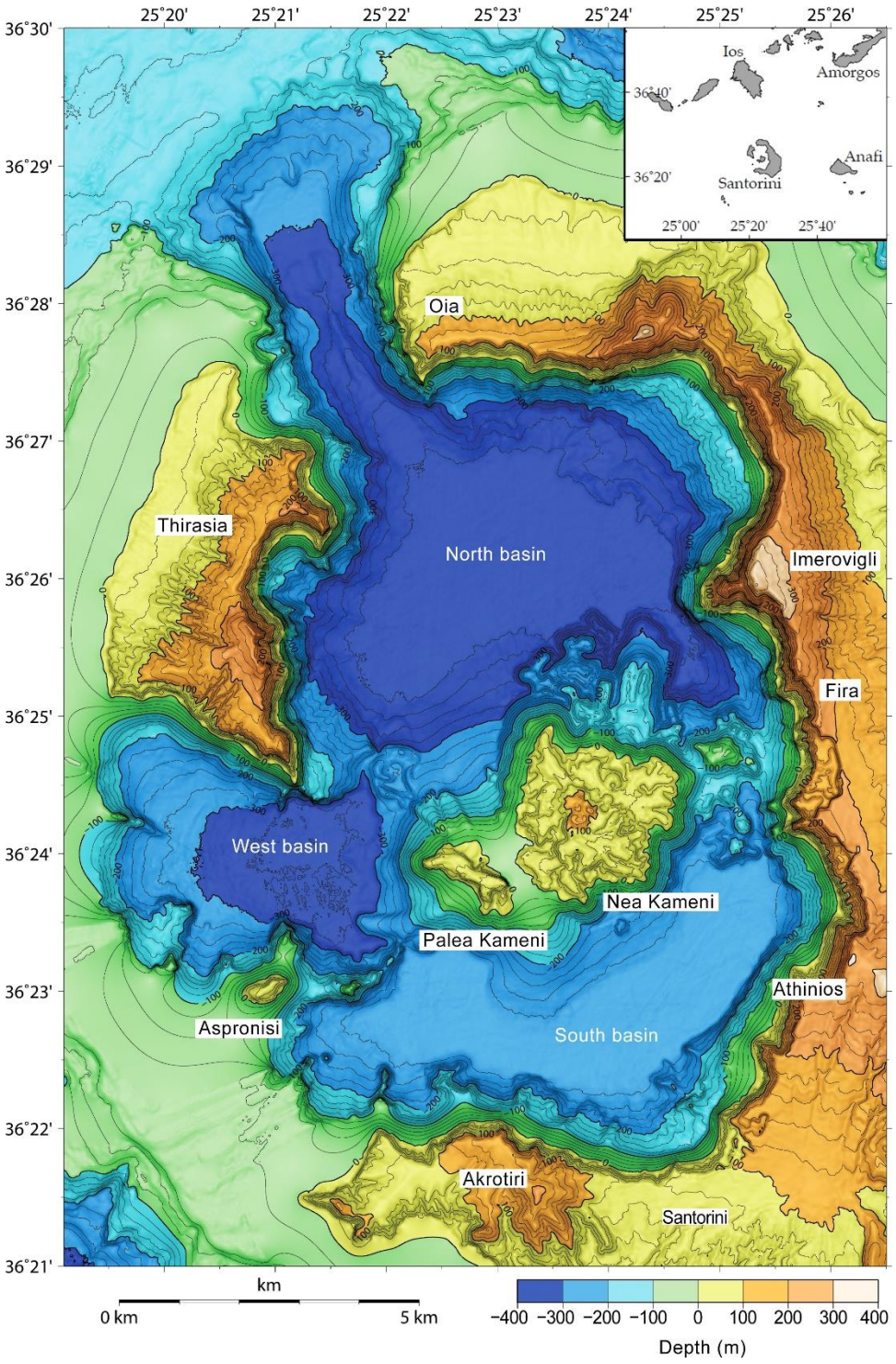

Fig.4: Combined bathymetric and topographic map of Santorini Caldera (Nomikou et al. 2014).

The morphology of the Santorini Volcanic Group is composed of: (i) the internal rocky and steep slopes of Thera, Therasia, and Aspronisi islands, forming the aforementioned caldera ring, characterized by high morphological dip values that approach vertical values in certain locations, and consisting of impressive morphological discontinuities, and (ii) the external sections of the islands, characterized by smooth surfaces of relatively low dipping angles and radial distribution to the volcanic centre, representing the remnant outer slopes of the volcanic cone (Fig. 5). The unique morphological plays an important role in landslide rockfall occurrence and determine the landslide hazard in a great extent (Fig. 6) (Antoniou & Lekkas 2010; Antoniou et al., 2017).

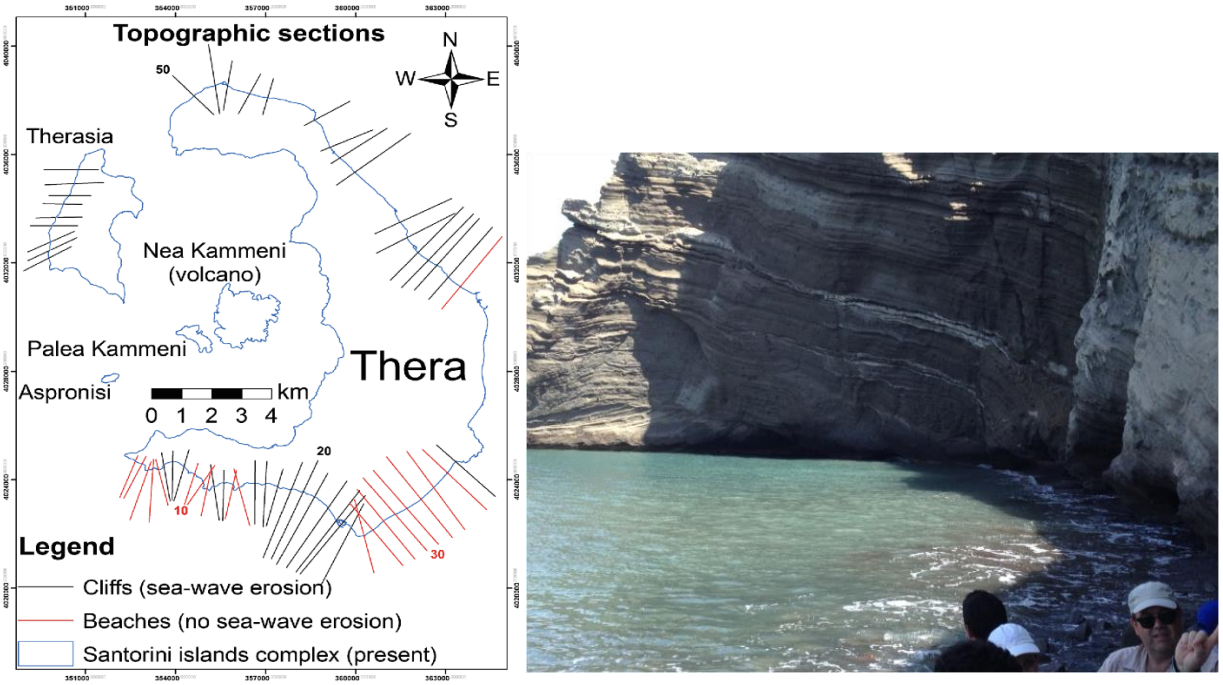

Fig.5: Left: Using topographic sections around the island, the 'missing parts' (sea-wave erosion) were calculated and the erosion rate was calculated (Oikonomidis et al., 2016). Right: photo from the coast of Kolumbo (photo: S.Pavlides).

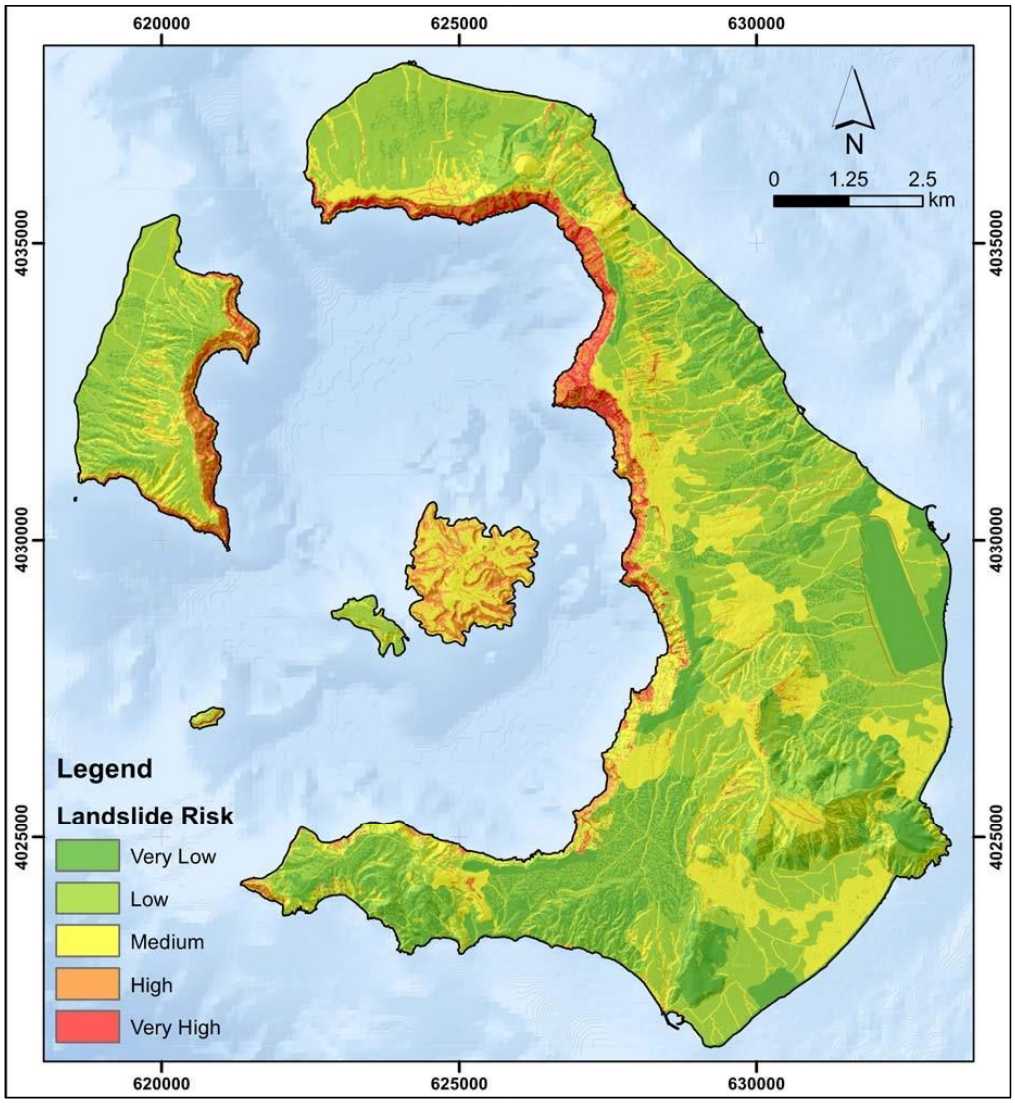

Fig.6: Landslide susceptibility map of the Santorini Volcanic Group. High risk values appear mainly into internal northern cliffs of Thera Island and the eastern ones of Thirasia Island due to lithology, slope, and land cover high risk values scattered along Thera's cliffs. Moderate to high values appear in Nea Kameni island (due to slope and lithology factors), along the caldera rim (due to land cover and road network factors) and scattered throughout Thera and Thirasia islands due to land cover and drainage network. The rest of the Santorini Volcanic Group displays Low and very low values (Antoniou et al., 2017).

1. Athinios Port (Basement lithologies)

Basement Lithologies

Athinios Port is located at the southern part of the caldera wall (inside the caldera ring) roughly between Fira (capital) and Akrotiri village (excavations). It is built on the basement metamorphic massif, which is part of the prevolcanic island that formed close to the nowadays center of

Santorini Island, from late Mesozoic to early Tertiary during the Alpine folding Orogeny (Fig.7). The metamorphic lithologies represented by low-grade phyllites (metapelites and schists) were found along the caldera wall at Athinios port but also at Profitis Ilias and Mesa Vouno mountains (IGME 1980; Kilias et al., 1998; Druitt and Davies 1999).

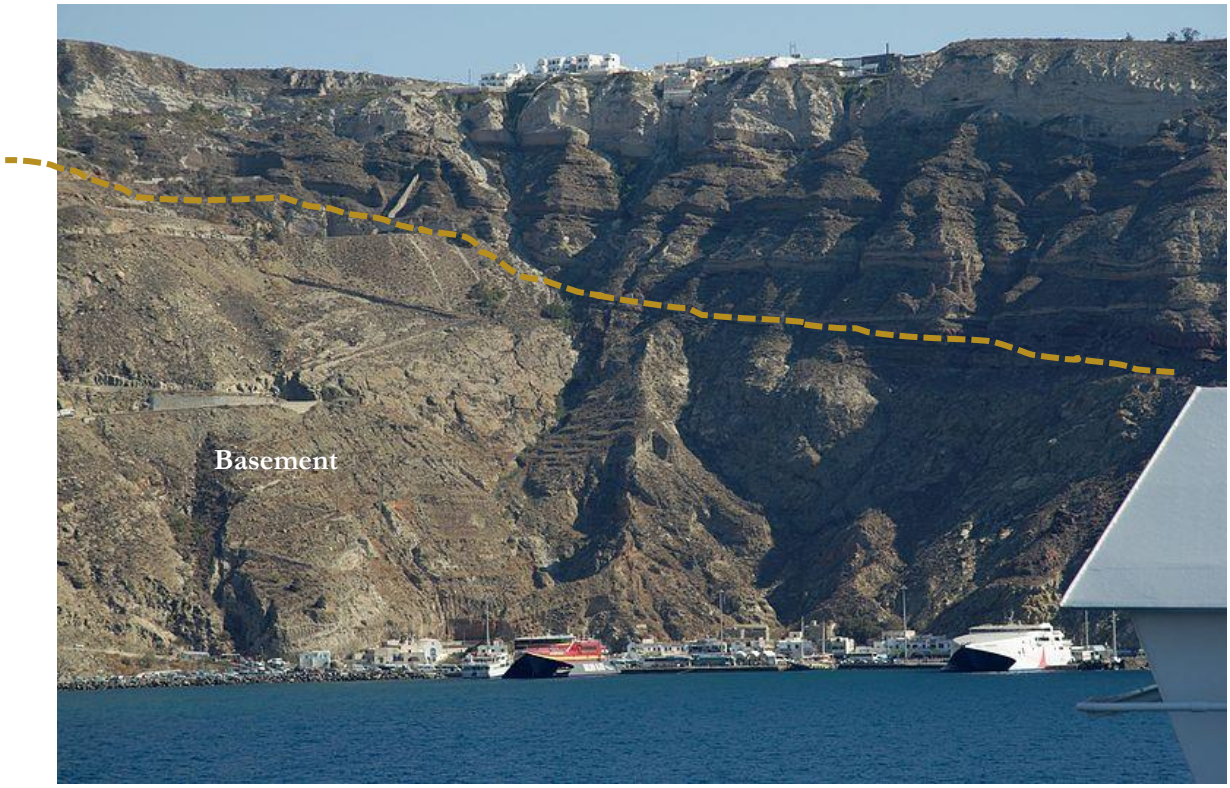

Fig.7: Location of basement lithologies at the Athinios port.

The metamorphic pathway (P-T path) is characteristic of the metamorphic facies of the typical subduction and exhumation processes influenced by (1) an Eocene high pressure blueschist phase followed by (2) an Oligocene-Miocene greenschist to amphibolite facies overprint (Barrovian metamorphic event, a sequence of regional metamorphic mineral reactions that form typical mineral assemblages) which was associated with a granitic intrusion (mostly about 20 - 9 Ma). The latter, which is part of the Cycladic Granitic Province, is the source of various ore minerals and it is observed at this spot.

The fabric that dominates the metamorphic rocks is a differentiated crenulation cleavage (schistosity) that indicates later deformation and metamorphism. In addition, a N-S lineation in schists is observed in the field scale (Fig. 8).

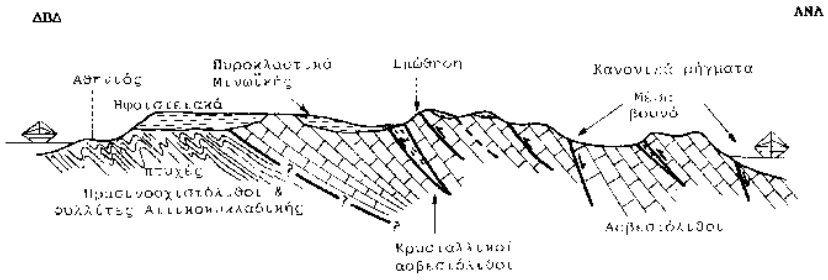

Fig. 8: A WNW – ESE schematic geological section from Athinios to Mesa Vouno. The basement rocks of the island are Phyllites - Green Schists - Crystalline Limestone) with their folds, thrusts and normal faults. On top of them are the newer volcanic rocks (Minoan pyroclastic mainly), (S. Pavlides), (Athinios port, Profitis Elias Mesa Vouno Green Schist Phyllites, Crystalline limestone, volcanic, thrusts normal faults).

2. Skaros shield-Therasia dome complex-Cape Riva eruption

Skaros shield

The Skaros shield atop the caldera that formed after the Middle Tuff eruptions (70-54 ka) and is observed in Therasia Island and extensively at Cape Tourlos. It is formed at the basement with silicic domes and coulees covered by well bedded mafic lavas. The same lavas are also found on the northern caldera wall (Fig.9).

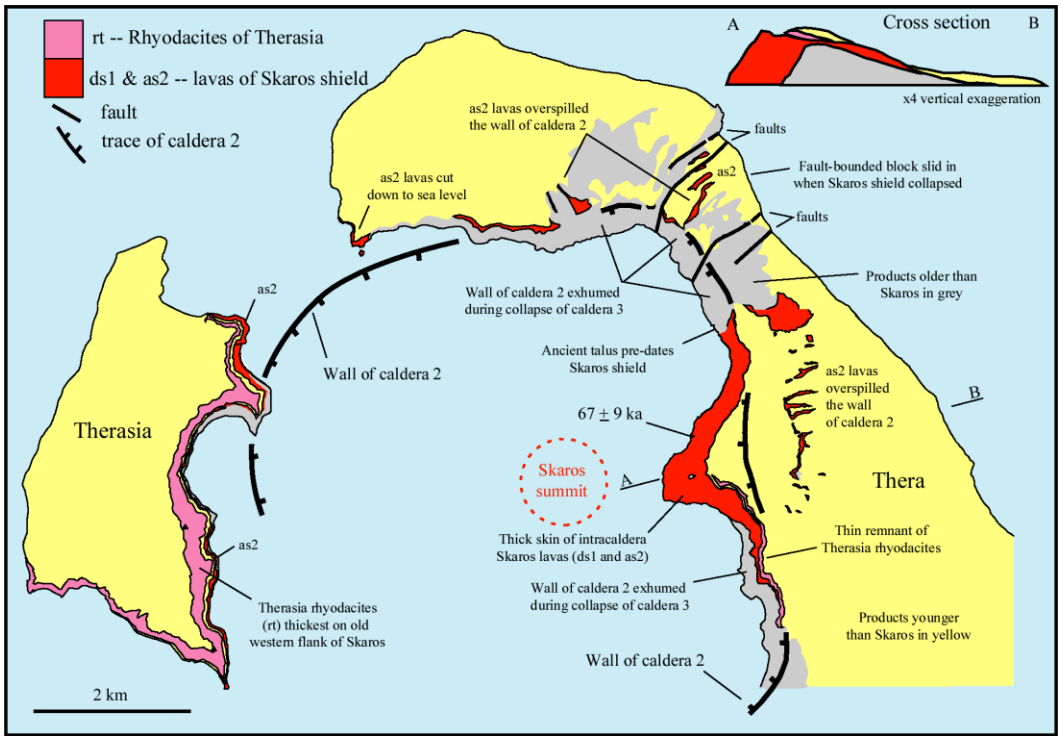

Fig.9: Present-day distribution of lavas of the Skaros and Therasia shields (Druitt et al., 1999).

The promontory at Skaros was inhabited during medieval times, because the fortress constructed there offered protection from pirates. Earthquakes during the eruptions of 1650 (Kolumbo), 1707 to 1711, and 1866 to 1870 hit the place hard and only few traces of the former buildings remain (Fig. 10).

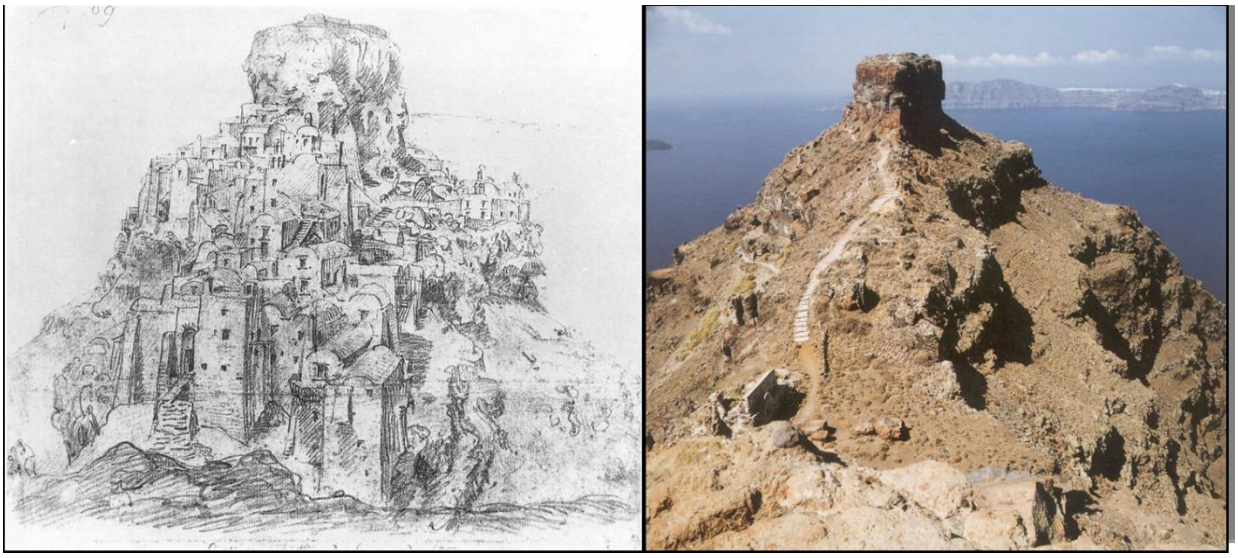

Fig.10: Right: Drawing by Fauvel from the book of Thomas Hope (1769-1831) "Images of 18th century Greece". Left: Skaros shield stratovolcano (present-day).

Therasia dome complex

Therasia dome complex is the western part of Santorini complex mainly influenced by the 70-21 ka volcanic activity. The stratigraphic sequence has been studied in detail by Fabbro et al., 2013 (Fig. 11). It is a succession of domes (dacitic) and flows (hybrid andesite) that dominates the cliffs of Therasia island and the top of the Fira cliff (Figs. 12, 13, 14).

Key Observations

- Unconformity (truncates LP2 and underlying units)
- Caldera collapse during the LP2.
- Volcanotectonic line (Kameni line) permeates the harbor into distinct morphologies (seismic epicenters during the 2011-12 unrest lay along that line)
- Landslides-Hazards

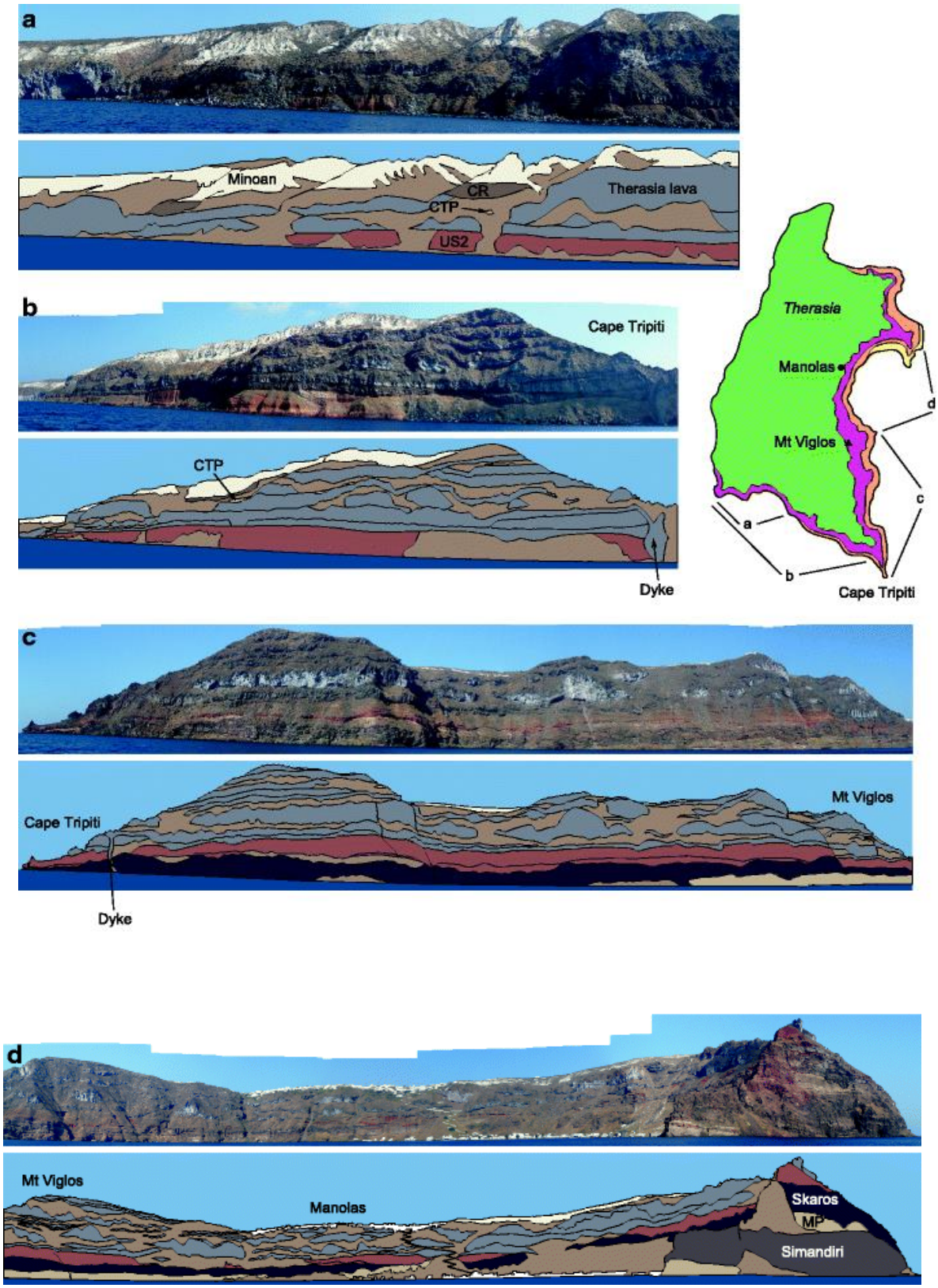

Fig. 11: Panoramic photos and sketches from the cliffs of Therasia (Fabbro et al., 2013).

Fig.12: Panoramic photo and stratigraphic interpretations of the Fira cliff (Simmons et al., 2017). According to the authors a Northward dipping unconformity is truncating the LP2 sequence, reflecting late-stage caldera collapse or post eruption slumping.

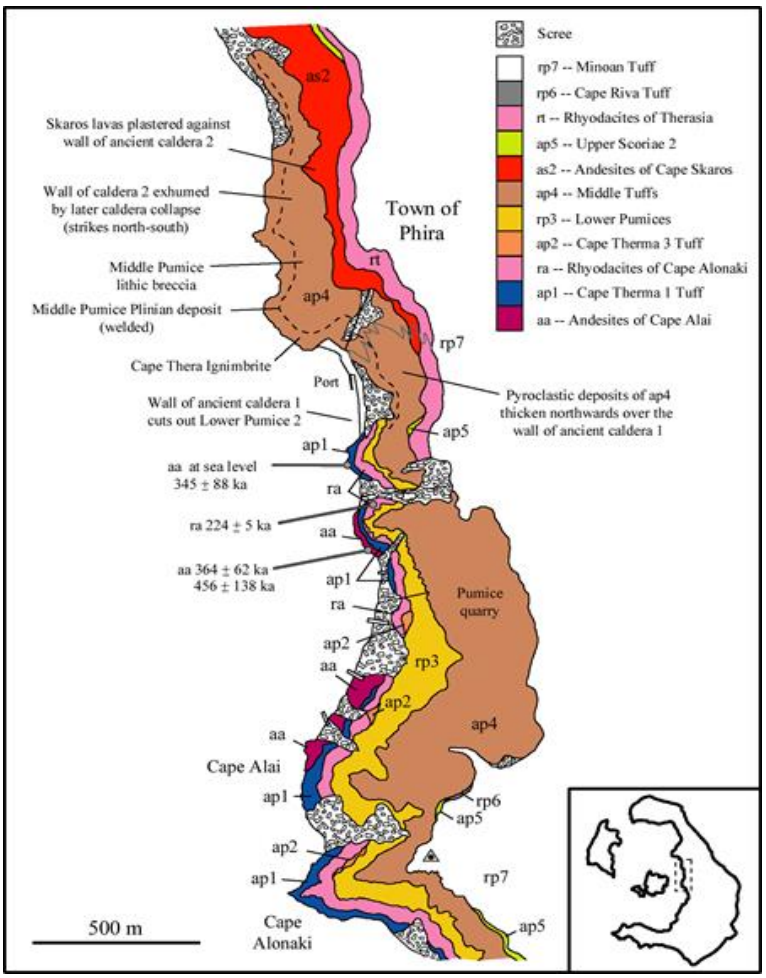

Fig.13: Geological map of Fira cliff (Druitt et al., 1999).

Fig.14: The Fira fault clearly observable on the Yalos port is a Normal Fault trending ENE-WSW. It was firstly drawn by the France expedition de Moree (1829-38). It shows gradually smaller Displacement from the see level to top lava layer (Nomikos Conference Center). Syn-volcanic fault growth (Pavlides & Chatzipetros, 2018).

Cape Riva eruption

It occurred at 22 ka and began with a pumice fall deposit that preserved mostly on the Northern caldera wall. As a continuation, a welded ignimbrite was emplaced over the island followed by second one (Fig. 15). The volume of magma discharged during the eruption is poorly constrained, as most of the ignimbrite lies under the sea. However distal tephra from the eruption, recognised as the Y-2 marine ash bed, is found over a very wide area of the eastern Mediterranean and as far north as the Island of Lesvos and the Sea of Marmara (Keller et al. 1978; Asku et al. 2008)

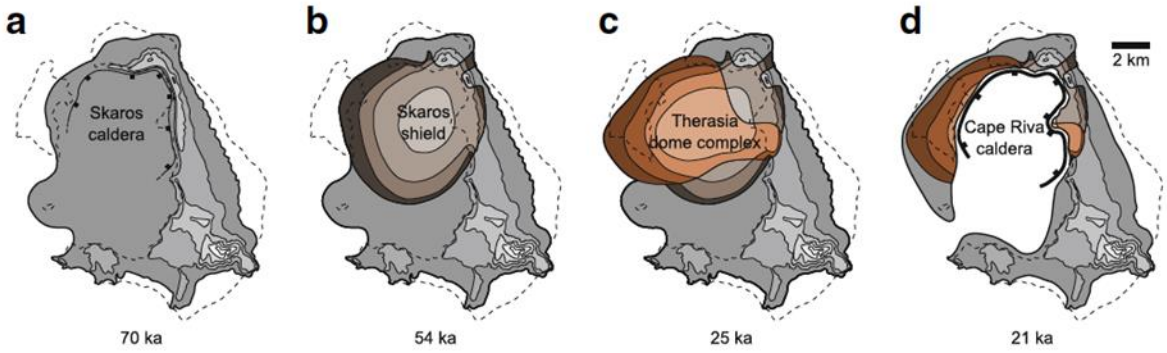

Fig. 15: Morphological evolution of Santorini between 70 and 21 ka, after Druitt et al., 1999.

3. Tectonics of the Island and the Northern caldera Dyke swarm

The crust of the Aegean is continental with thicknesses in the range of 20-32 km. Most of the tectonic lines seen both on Santorini and on seismic profiles follow the general southwest-northeast trend (Hofft et al., 2017). Onland neotectonic faults are normal directed mainly NNE-SSW to E-W (see neotectonic map, Fig. 16, Mountrakis et al., 1998). The most important tectonic structure is close to cape Kolumbo (northern Santorini), part of the greater Kolumbo

line, where meso scale faults and many fault associated dykes (~60) are observed and measured at the caldera wall (Mountrakis et al., 1998).

Dyke or (dike) is a fluid driven (magma driven) extension fracture (mode I) that if it reaches the surface as a feeder (dyke) it feeds a volcanic eruption but if it became arrested on the way to the top, a volcanic eruption is suspended. A dyke-fracture is almost entirely forced to propagate by the overpressure of the magma.

Recent studies have shown that the dyke swarm is emplaced in a highly heterogeneous host rock made up of many layers of contrasting mechanical properties; for example, stiff lava flows and comparatively compliant layers such as ash, volcanic tuffs and breccia. A total of 91 dykes has been recently mapped and structurally studied showing that the majority of the dykes have been arrested due to changes of the stress field during their emplacement and only a few of them probably fed (or not) a volcanic eruption (Browning et al., 2015) (Fig. 17).

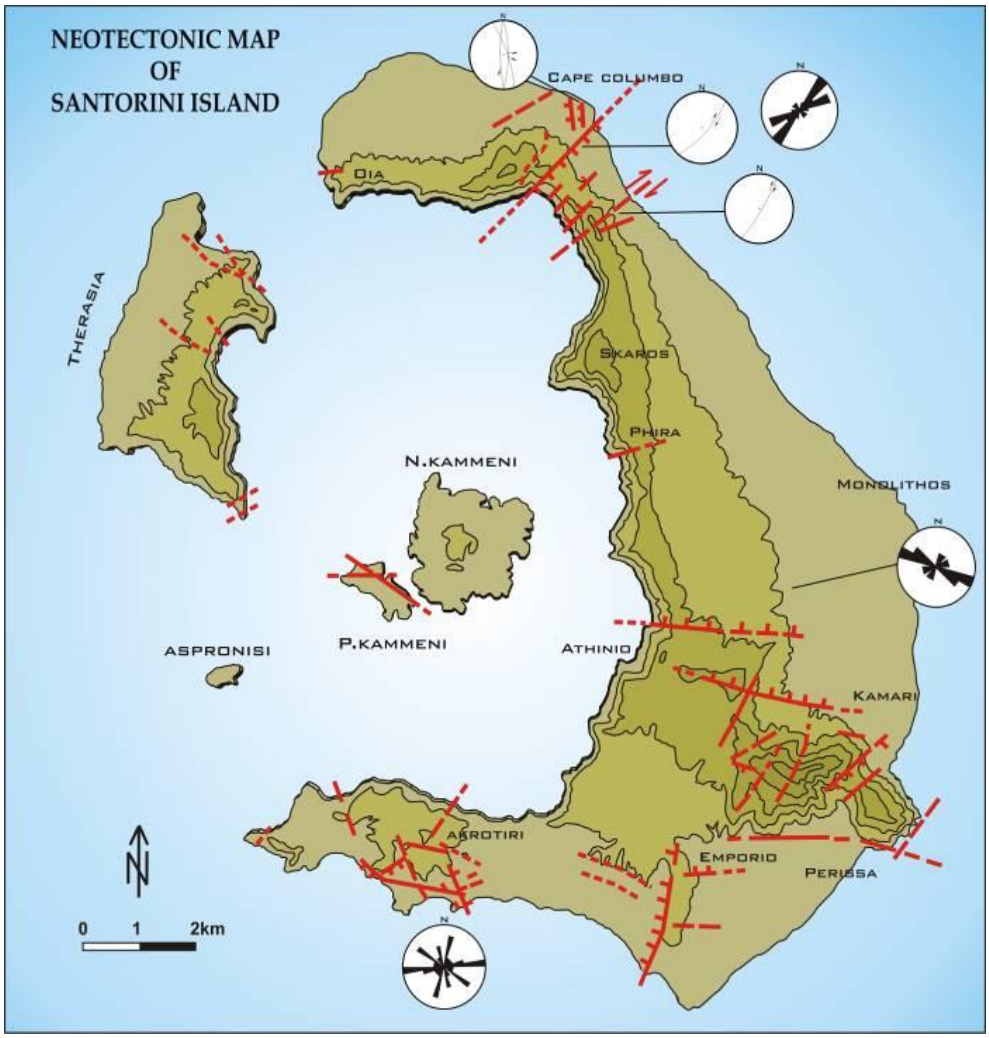

Fig.16: Neotectonic map of Santorini Island group (Mountrakis et al., 1998).

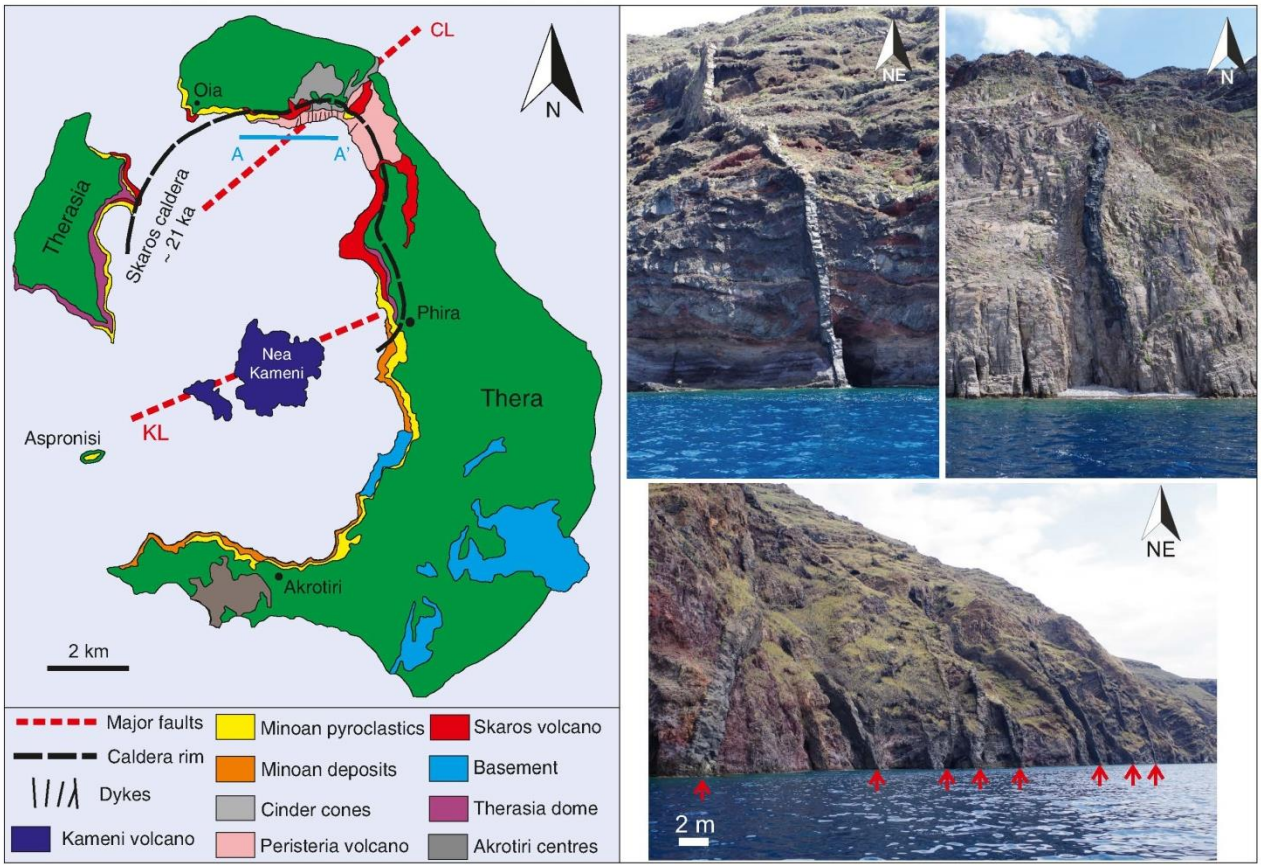

Fig.17: Simplified geological map of Santorini, showing the two main tectonic elements: the Kameni and Kolumbo lines, the inferred Skaros caldera rim, and the location of dykes within the northern caldera wall (schematic). All the exposed dykes are located along the northern most extent of the Skaros caldera wall and the island of Therasia; some are marked in the figure with red arrows. Most dyke measurements were taken from a boat along the profile A – A'. The stratigraphy of the caldera is complex, being made up of many different types and ages of deposits. Many dykes within the wall are arrested, i.e. are non-feeders (Browning et al., 2015).

4. Red Beach

Red Beach is one of the most famous beaches within the Aegean and Mediterranean Seas due to its particular colour, its particularly beautiful geomorphological environment, and its proximity to the remarkable archeological site of Akrotiri. The length of the beach is approximately 300 m, while its width varies from 4 to 10 m, and it is strongly affected by sea erosion (Fig. 18). Rock falls are generally frequent. According to Druitt and Francaviglia (1992) and Friedrich (2000), the area of Akrotiri was the first instance of volcanism on Santorini Island and was formed exclusively by dacitic and andesitic volcanic products of the Pre-Minoan eruption era. Late-Pliocene to 580 ka silicic volcanism constructed a complex of domes, hyaloclastite aprons, and pumice cones on the western submarine flank of the pre-volcanic island. Later stages in the development of the complex were probably subaerial, suggesting shoaling during construction. Subsequent uplift of the complex occurred as two fault blocks. Uplift was probably complete by the time the subaerial cinder cones of Mavrorachidi (522+104 ka) erupted. Strombolian eruptions

on the Akrotiri Peninsula between ~350 and ~520 ka formed cinder and spatter cones at Capes Balos, Kokkinopetra, and Mavrorachidi. All three cones overlie tuffs and lavas of the early rhyodacitic centres, but underlie the Thera pyroclastics.

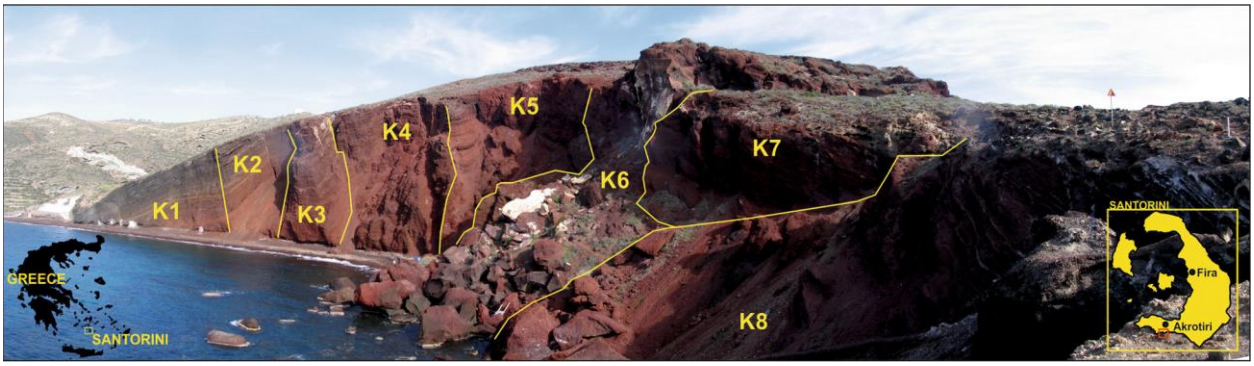

Fig.18: Location and view of the Red Beach cliffs, where rock falls present with episodic characteristics. The zonations (K1–K8) used to delineate rockfall potentials are illustrated (Marinos et al., 2017).

5. Metaxa Mine –Vlychada (Minoan phases)

The Late-Bronge-Age Eruption

The Late-Bronze-Age, known as "Minoan" eruption of Santorini may have influenced the decline of the great Minoan civilization on Crete, making it an iconic event in both volcanology and archaeology (e.g., Manning et al. 2006, Druitt 2014). It has been dated by the ^{14}C method on short-lived samples (seeds, twigs) preserved in the Bronze - Age town of Akrotiri (1660–1613 BC; Manning et al. 2006; 95 % confidence limit) and by ^{14}C wiggle-match dating of an olive tree buried in the plinian fall deposit (1627–1600 BC; Friedrich et al. 2006; 95 % confidence limit). Insect death assemblages constrain the eruption month to June or early July (Panagiotakopulu et al. 2013). The eruption impacted the late-Bronze-Age Mediterranean world through a combination of ash fallout (Pyle 1990, Johnston et al., 2014), climate modification (Pyle 1997), and tsunamis (Bruins et al., 2008).

The 'Minoan' eruption was the last plinian eruption of Santorini (Sparks and Wilson 1990; Druitt 2014; Cadoux et al., 2015). It discharged between 30 and 80 km^3 (dense-rock equivalent; Johnston et al. 2014) of rhyodacitic magma, mostly as pyroclastic flows which entered the sea and which are preserved as ignimbrite in the surrounding submarine basins (Sigurdsson et al. 2006). According to numerous volcanological studies, there is a consensus that the eruption occurred in four major phases with an initial precursory phase (P0) (Heiken & McCoy 1990; Druitt 2014) (Fig. 19).

Metaxa Mine-Story maps

https://nom.maps.arcgis.com/apps/Cascade/index.html?appid=2a6c54875bf743dd8143786a55dcb2b1&fbclid=IwAR3icBFUBjoKLde--YcQ54tvYpjNR57cL6X73UUBnQ_Aj4f4LNwU7eWBKEQ

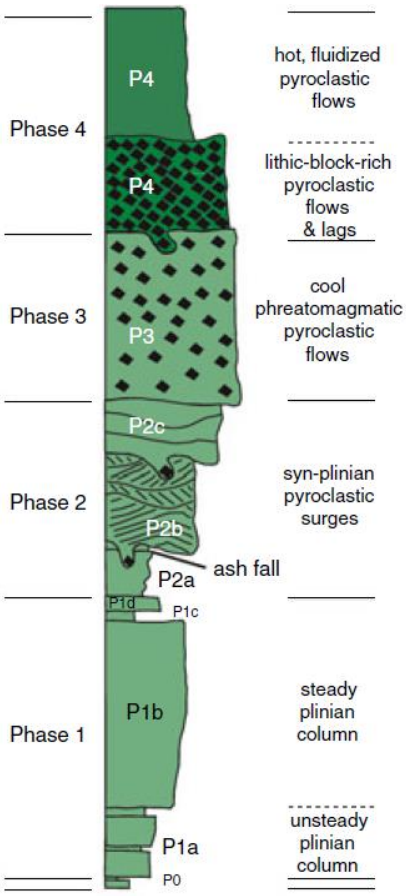

Fig.19: Four phases of the Minoan eruption (Druitt 2014).

Minoan Phases

Phase 0

The eruption began with precursory explosions that left two lapilli fallout layers and a phreatomagmatic ash totaling 10 cm in thickness (Heiken and McCoy 1990; Cioni et al., 2000). Druitt (2014) call these explosions eruptive phase 0 (Fig. 20). Cioni et al (2000) estimated that the two lapilli layers were laid down from a subplinian plume 7–10 km high. The plume was blown to the SSE, so that P0 is restricted to that sector.

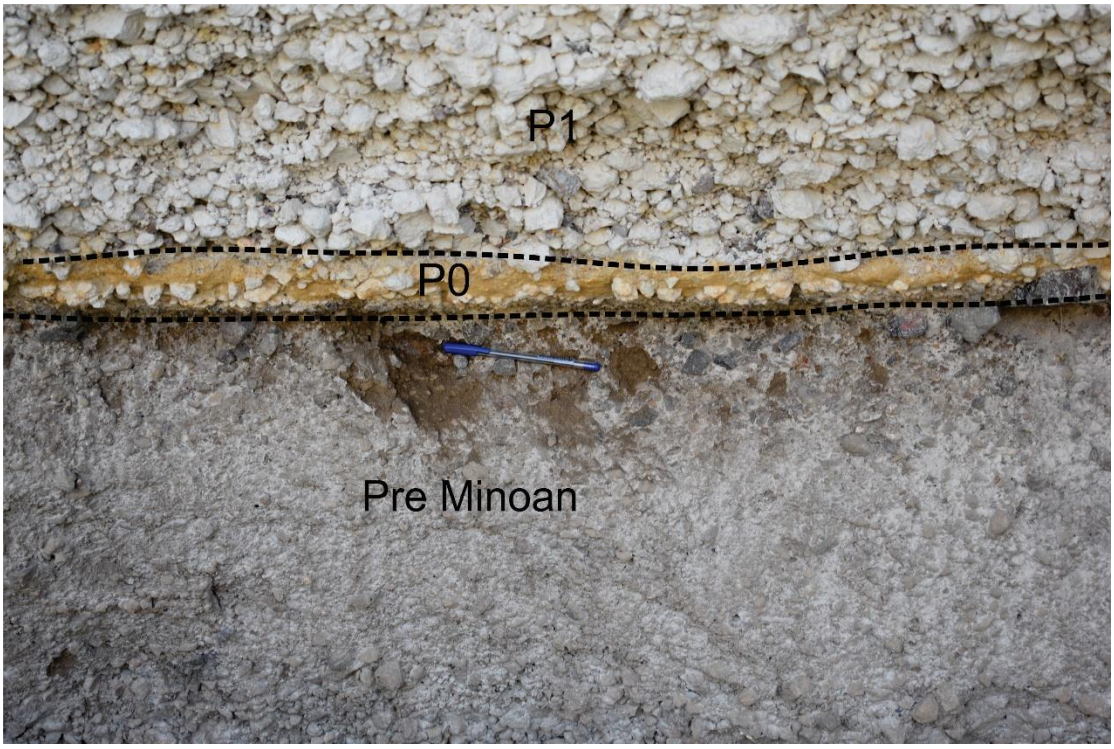

Fig.20: Base of the Minoan eruption sequence in Metaxas quarry showing products of phases P0 and P1a, as well as the pre-Minoan volcanic (Riva) and the Minoan age palaeosoil including ceramic fragments (photo: P. Nomikou).

Phase 1

The first main Plinian eruption (Phase 1; Fig. 21, Johnston et al., 2014) generated a sustained plume estimated at a height of 36 ± 5 km and produced a reverse-graded pumice fall deposit that ranges from 6 m to less than 10 cm in thickness on the islands of Santorini, Therasia and Aspronisi (Bond & Sparks 1976; Sparks & Wilson 1990; Sigurdsson et al. 1990).

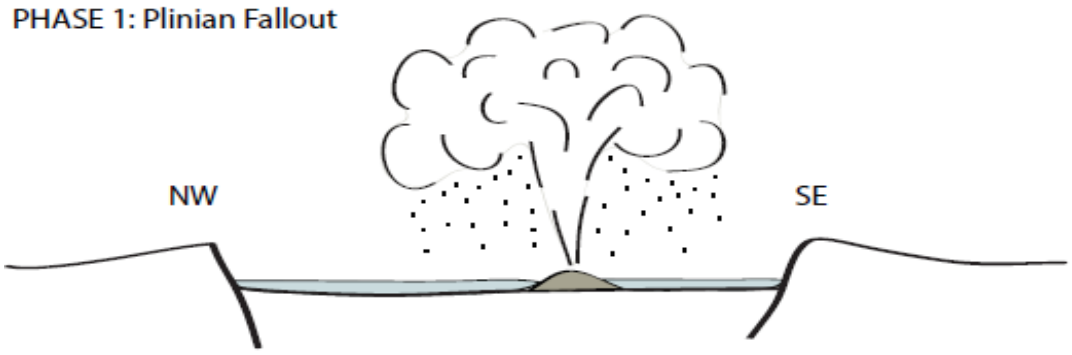

Fig.21: Schematic illustration of Phase 1, Plinian fallout (Johnston et al., 2014).

The deposit has, from the base upwards, a reversely graded, crudely bedded unit (P1a) overlain by a coarser, unbedded unit that is normally graded in its upper part and contains up to a few percent of andesitic scoria (P1b) (Druitt 2014) (Fig. 22).

Fig.22: Phase 1 and 2 deposits in Pyrgos quarry bordered by a dotted line (Photo: P. Nomikou).

Phase 2

During Phase 2 (Fig. 23, Johnston et al., 2014), access of seawater to the vent initiated violent phreatomagmatic explosions and triggered the generation of base surges that spread radially away from the vent, and formed stratified deposits up to c. 12 m thick (Sparks & Wilson 1990).

Fig.23: Schematic illustration of Phase 2, Base surges (Johnston et al., 2014).

The phase 2 products are dominated by pyroclastic surge deposits with multiple bedsets, dune-like bedforms with wavelengths of several meters or more, bomb sag horizons, and TRM temperatures of 100–250 °C (Bond and Sparks 1976; Heiken and McCoy 1984; McClelland and Thomas 1990). The lowest bedset, P2a, is fine-grained and contains accretionary lapilli. The overlying sequence of multiple bedsets (P2b) is much coarser grained than P2a and contains lenticular layers of surge-reworked plinian fallout pumice, showing that the P2b surges were synplinian (Fig. 24).

Fig.24: The dotted line marks the boundary between Phase 2 and 3 deposits in Mavromatis (Metaxas) quarry (*Photo: P. Nomikou).*

Phase 3

During Phase 3, increasing water–magma ratios produced denser, partly wet, low-temperature pumiceous pyroclastic flows transitional to mud flows. These deposits formed a fan of numerous amalgamated single flow deposits as opposed to one giant, massive flow (Fig. 25, 26) (Johnston et al., 2014, Sparks & Wilson 1990, Pfeiffer 2001).

In the third phase, significant column collapse produced the most prominent unit of the eruption on land. This is a coarse-grained, massive, phreatomagmatic ignimbrite up to 55 m thick (Druitt et al., 1999), still reflecting magma-water interaction and deposited at low temperatures (Druitt, 2014, McClelland E. & Thomas R. A.1990). The third eruptive phase may have created a tuff cone (Nomikou et al., 2016), possibly a large pyroclastic construct filling the caldera bay (Fig. 20, Johnston et al., 2014). This phase is thought to coincide with the explosive disruption of the Pre-Kameni island (along with other parts of Santorini), given the occurrence of abundant, evenly distributed lithic clasts up to 10 m in size in the deposit (Karatson et al., 2018).

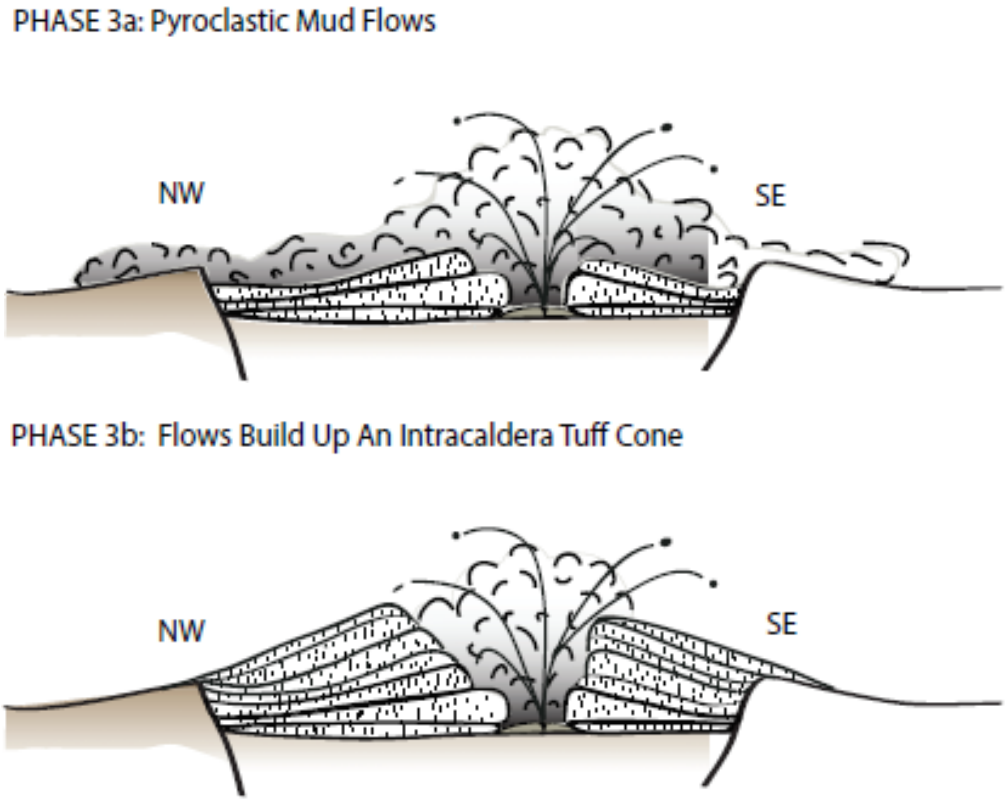

Fig.25: Schematic illustration of Phase 3, Pyroclastic mud flows/flows build up an intercaldera tuff cone (Johnston et al., 2014).

The P3 ignimbrite is massive to crudely bedded, with multiple flow units. Lithic blocks up to a meter or more in diameter are common. P3 has been interpreted as the deposit from low-temperature, three-phase (solid, gas, water) cohesive pyroclastic flows, with subordinate ballistic, surge, mudflow, and slump facies (Heiken and McCoy 1984; Sparks and Wilson 1990).

Fig.26: The products of Phases 1 to 3 in Fira Quarry (*Photo: P. Nomikou).*

Phase 4

Phase 4 (Fig. 27, Johnston et al., 2014) saw the venting of high-temperature (300–500 °C) pyroclastic flows, which produced fine-grained, nonwelded ignimbrites around the caldera rim and the coastal plains (Bond & Sparks 1976, Heiken & McCoy 1984, Sparks & Wilson 1990, Druitt et al. 1999).

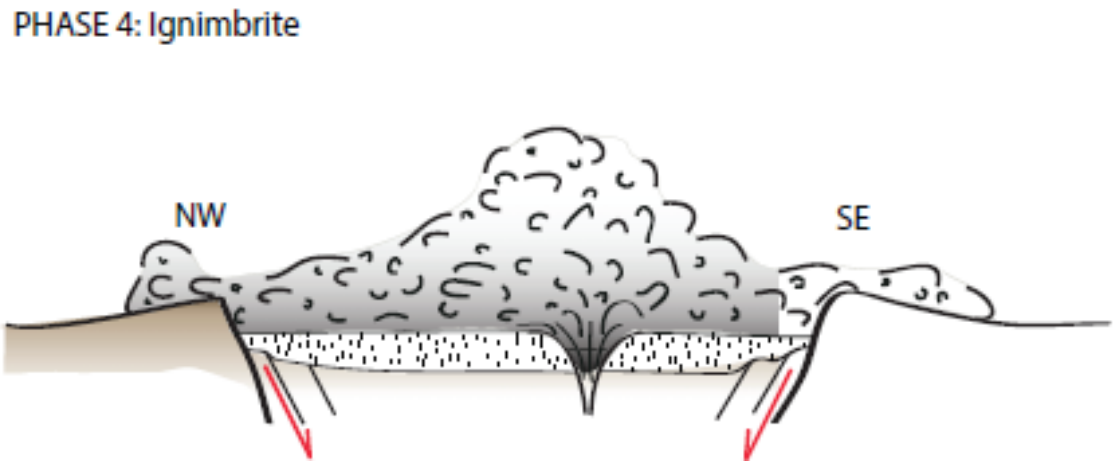

Fig.27: Schematic illustration of Phase 2, Base surges (Johnston et al., 2014).

The dominant facies is a tan-to pink- colored compound ignimbrite ("tan ignimbrite") (Druitt, 2014). The ignimbrite is mostly finegrained (ash and lapilli grade), with a high abundance of comminuted lithic debris in the ash fraction (Bond and Sparks 1976). This phase may have been coeval with major caldera collapse (Sparks & Wilson 1990, Druitt, 2014). Minoan ignimbrite, possibly up to 80m thick, lies offshore of Santorini (Sigurdsson et al., 2006) and is the most voluminous Minoan unit (Fig. 28).

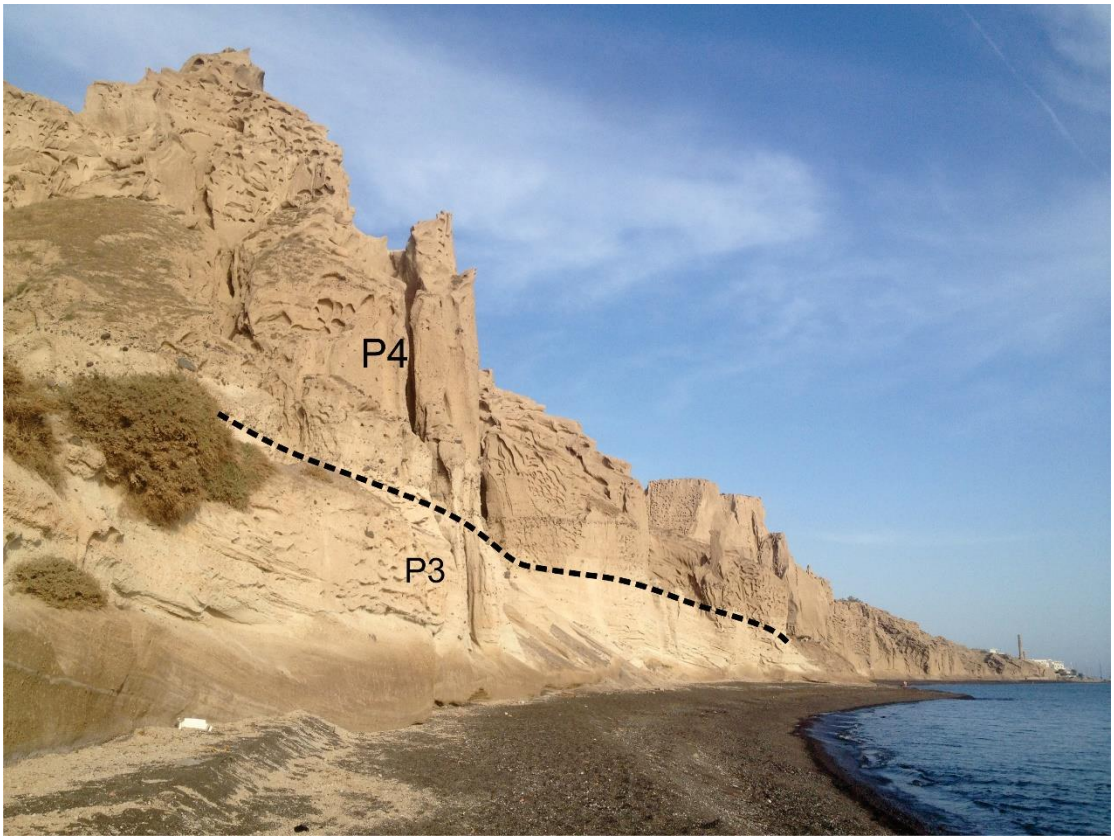

Fig. 28: Typical P4 tan ignimbrite of the S fan in Vlychada; cliff 40 m high (*Photo: P. Nomikou).*

Pumice fall temperature

Rock magnetic and palaeomagnetic analyses on palaeosoil ceramic fragments from Megalochori (Metaxas) Quarry and lithic clasts collected from the pumice fall deposited inside the archaeological site of Akrotiri have been applied in order to estimate the deposition temperature of the first volcanic products of the Minoan eruption. All samples have been stepwise thermally demagnetized and the obtained results have been interpreted through principal component analysis. The equilibrium temperature obtained after the deposition of the pumice fall varies from sample to sample but generally shows temperatures around 240º-280º C. The temperature data show that the pumice fall was still relatively hot when deposited inside the archaeological site as well on Minoan palaeosoil and even if it interacted with the buildings, often causing the

collapse of roofs, it still remained hot with mean temperature around 260° C (Tema et al., 2013; 2015).

Tsunami generation

Minoan culture in the southern Aegean region through damage to coastal towns, harbours, shipping and maritime trade (Marinatos 1939, McCoy & Heiken, 2000, Novikova et al., 2011). Evidence for regional tsunamis generated by the LBA eruption has been reported from deep sea megaturbidites (Cita M. B. 1997; Cita M. B. & Aloisi G. 2000; Rebesco et al., 2000) and from sediment layers at or near the coasts of Santorini, northern Crete, west Turkey and Israel (Minoura et al., 2000; Bruins et al., 2008). Prior to the LBA (Minoan) eruption there existed an ancient caldera in the northern half of the volcanic field (Athanassas et al., 2016; Druitt & Francaviglia, 1992). This caldera was lagoonal, as shown by the presence of fragments of ancient travertine, stromatolites (Fig. 29) and brackish to marine fauna in the LBA ejecta (Eriksen et al., 1990; Anadon et al., 2013). There was also an andesitic edifice within this caldera (Druitt, 2014).

Fig.29: Stromatolite of the pre-Minoan lagoonal caldera at the northern part of the Island. (Photo S. Pavlides). Their analysis showed that probably in the northern basin a shallow sea-flooded lagoon existed before the eruption where these stromatolites grew. (Eriksen et al., 1990).

In eruptive phase 1, a Plinian eruption took place, which in phase 2 was joined by the production of syn-plinian pyroclastic surges. In phase 3, eruption of 'cold' phreatomagmatic pyroclastic flows constructed a large tuff cone that filled the old caldera, cutting it off from the sea. In phase 4, eruption of hot pyroclastic flows took place from multiple subaerial vents, forming at least three ignimbrite fans (NW, E and S), and associated caldera collapse enlarged and deepened the ancient caldera. The main eruptive vents are shown in Fig. 30 as red stars (locations well constrained for phases 1 to 3, but speculative for phase 4). Black arrows show schematic

emplacement vectors for the pyroclastic flows of phases 3 and 4 (d-e). Post-eruptive opening of the NW and SW straits (Nomikou et al, 2016). According to Nomikou et al., 2016, at the end of the eruption the caldera was dry and isolated from the sea, probably due to thick accumulations of LBA tuff. The sea first broke through to the NW, where a combination of water erosion and landslip carved out the NW strait and flooded the caldera (blue arrows in d) in less than a couple of days. Submarine landslides (black arrows in e) then opened up the SW straits once the caldera was largely flooded. The regional-scale tsunamis associated with the LBA eruption were generated by the pyroclastic flow inundation of eruption phases 3 and 4, augmented perhaps by mass slumping of rapidly deposited pyroclastic deposits off the seaward slopes of the island volcano (Nomikou et al., 2016). This is consistent with tsunami modelling that shows that pyroclastic flows were indeed capable of generating waves of the observed height in northern Crete. It is also consistent with previous assertions that pyroclastic flows were the main cause of tsunamis at Krakatau (Paris et al. 2914).

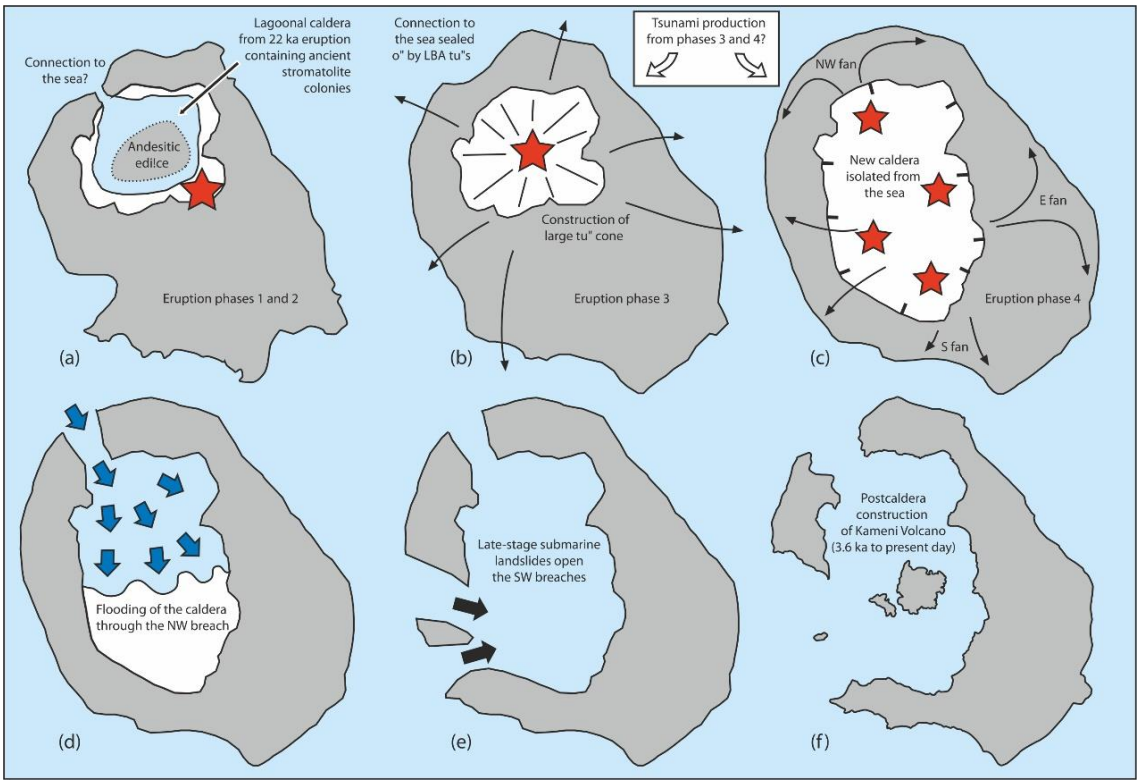

Fig.30: Tsunamis generated by the eruption of Santorini in the late Bronze Age may have been generated by the entry of flows of volcanic material into the sea (Nomikou et al. 2016).

Dating the great Minoan eruption

The Minoan eruption is a key marker for the Bronze Age archaeology of the Eastern Mediterranean world. The eruption has been difficult to determine. For most of the twentieth century, archaeologists placed it at approximately 1.450 to 1500 BC, but this date appeared to be too young as:

- Greenland ice cores show evidence of a large volcanic eruption in 1642 ± 5 BCE which has been associated with Santorini. However, volcanic ash retrieved from an ice core does not match the expected Santorini fingerprint
- Radiocarbon dating analysis of an olive tree buried beneath a lava flow from the volcano indicates that the eruption occurred between 1627 BCE and 1600 BCE with a 95% degree of probability (Friedrich, et al. 2006).

So, Santorini Eruption Radiocarbon Dated to 1627-1600 B.C suggest an eruption date more than a century earlier than suggested by archaeologists (Fig. 31).

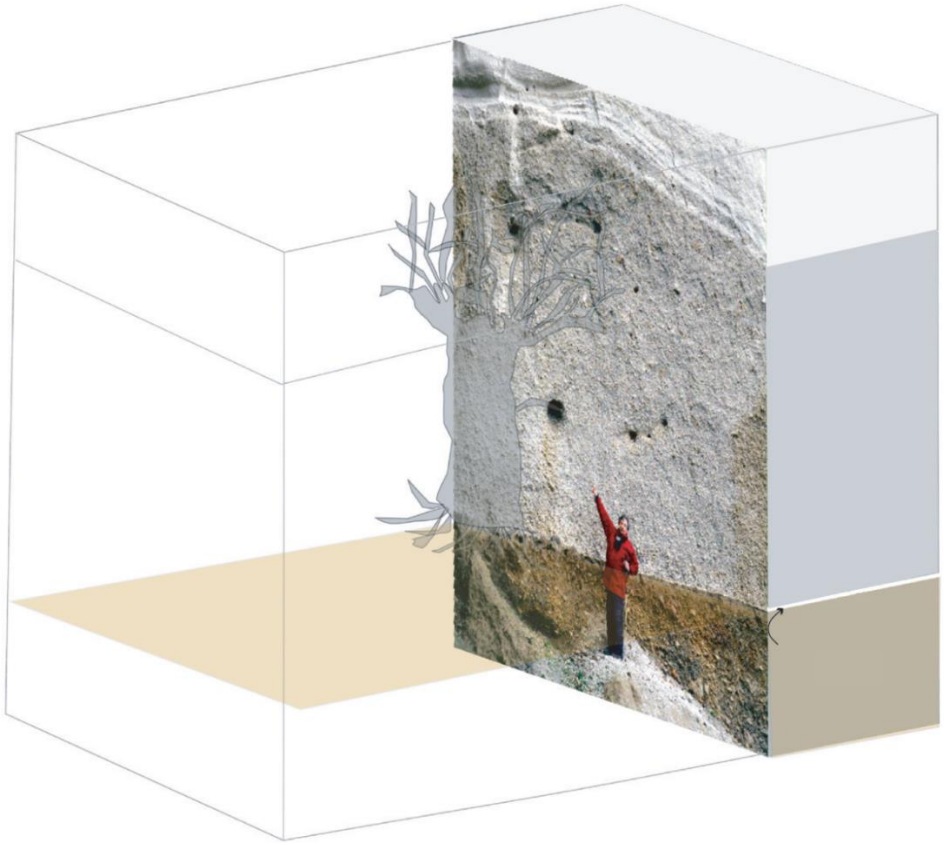

Fig.31: Picture of the olive tree in situ, buried beneath the the 1st and 2nd fall and surge flow phases of the Late Bronge Age eruption (Minoan) (Friedrich, et al. 2006).

6. Akrotiri Excavations

In 1856 construction of the Suez Canal between the Mediterranean and the Rad Sea began. During its construction, pumice was mined in Santorini for the cement mixture used in the concrete lining the canal. The quarrying of pumice on Santorini was a big business, but it revealed prehistoric structures, first on the island of Therasia (the westernmost of the islands of Santoirni) and later on Thera. The Therasia ruins were first studied by F. Lenormant in 1865, and later by French geologist Ferdinand Fouqué in 1867. In 1869 Fouqué also made a major discovery near Akrotiri, and concluded that the site had been buried by an eruption between 2000 and 1300 BC, which is a pretty good estimate at the time! Fouqué had to stop his excavations

because of the Franco-Prussian war in 1870, but in 1879 he published his classic work *Santorin et ses Eruptions*.
Near the village of Akrotiri, a peasant showed Fouqué an ancient wall fragment that rose out of a ravine in the pumice deposits. After a little digging, he recoverd a wealth of pottery and many other artefacts. Fouqué had clearly discovered a town, but did not have time or resources to continue his work here. The Greek archaeologist Spyridon Marinatos began the excavations at Akrotiri in 1967, opening a new chapter in the history of Aegean archaeology. His theory was that the decline of the Minoan civilization was due to the eruption of the Thera volcano, and he set out to prove it at Akrotiri, which is being questioned recently, after the new and extensive excavation of the C. Doumas team and new dating of the eruption (Doumas 1983).

These still ongoing excavations at Akrotiri have brought into light an immense volume of finds, the study of which has provided important information, very often leading to revision of many old views about the early history of the Aegean. It is now an undisputable fact that the site of Akrotiri was inhabited since the middle of the 5th millennium BC. At the dawn of the 3rd millennium BC the small coastal settlement was already in the orbit of the Early Cycladic culture taking an active part in its formation. As the plethora of Early Cycladic culture and Akrotiri was developing into an important commercial port. In the late 3rd or the early 2nd millennium BC a major program of town planning promoted Middle Bronze Age Akrotiri into a great urban center of cosmopolitan character and to the sophistication of its culture (Fig. 32).

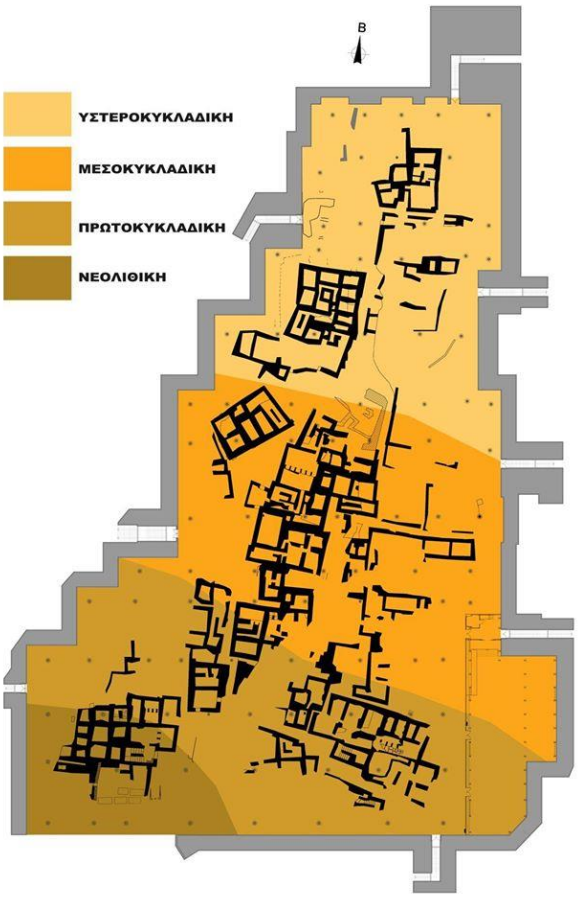

Fig.32: A map of the excavations of Akrotiri, after Doumas 1983. Only a portion of the town has been excavated so far.

Craft specialization and division of labor, which are reflected in the products of the material culture (pottery making, metalworking, shipbuilding) bear witness to the urban character of Theran society, a character which is confirmed by the multistoried mansions with their impressive sanitary, installations, rich household equipment and exquisite pieces of furniture. The unique wall paintings recovered from the ruins of these residences not only constitute an inexhaustible source of information about the daily life, activities and appearance of Akrotiri's inhabitants, but are also works of high art. This art was enjoyed by individuals, citizens, the very creator of the wealth and the culture that generate it: merchants, sailors, artisans. The great eruption of the volcano, round the middle of the 17th or 16th century BC, brought this thriving "bourgeois" society to an abrupt end (Fig. 33).

Fig. 33: view of a typical house in the Akrotiri excavations (photo: P.Nomikou).

The area had been continuously inhabited since the neolithic period, until a tremendous volcanic eruption covered everything the islanders had created with a layer of pumice and ashes. The architecture of the city is strongly Cycladic. The houses were two - or three - storeys high with many rooms (Fig. 34). The most luxurious houses were built of moulded stone; the others were made of mud and straw. No written documents of any kind have been found in the prehistoric city of Akrotiri. This means that, in order to be able to get some picture of economic and social life before the catastrophe, scientists had to rely solely on the rich findings unearthed by the digs. The reputation of the Cycladic islanders as seafarers as well as scenes in frescos, showing naval fleets, led to the conclusion that the citizens of Akrotiri must have had a flourishing merchant navy (Fig. 35). This would have allowed them to maintain trade with Crete and the mainland of Greece. Natural scenes in the frescos show subjects that are not native to Greece, but rather seem related to the landscape of Egypt indicating that the islanders also had contact with that region. The large number of vases and other types of pottery tell us that another flourishing sector of the island's economy was that of ceramic production.

The finding of stone tools and vessels, such as mills, pestels and hammers, implies a well developed form of masonry. Finally, the high quality of town planning, architecture and painting shows that Santorinians of that period were superb architects, constructors, engineers and artists.

Fig.34: Triangular Square with West House to the left (photo: P.Nomikou).

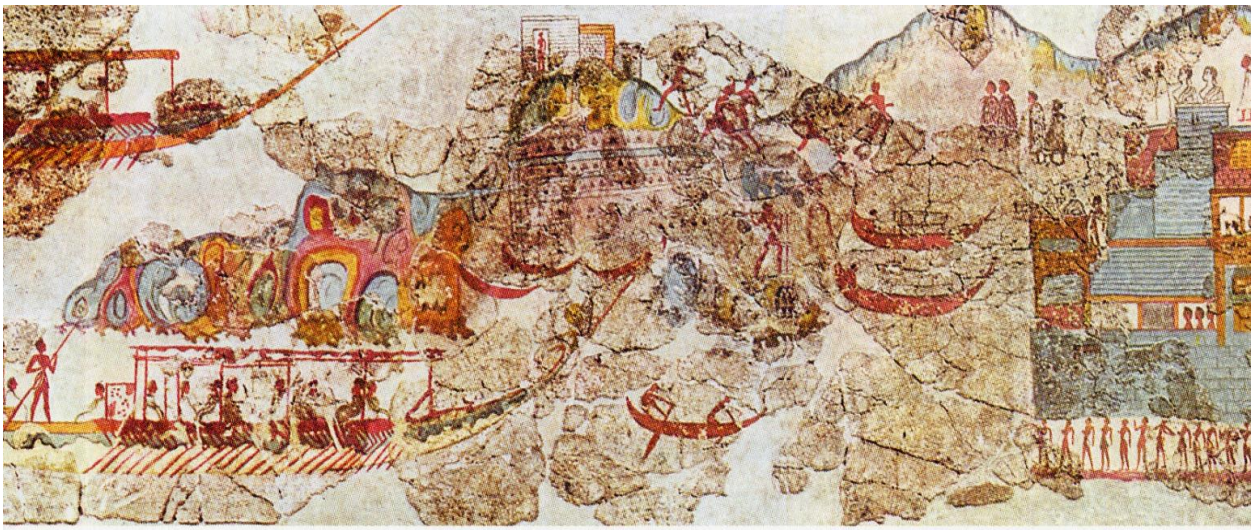

Fig.35: West House Miniature Fresco ('Arrival Town').

7. Nea Kameni & Palaea Kameni-Santorini Unrest-Amorgos eartquake

Eruption History

A possible third eruptive cycle of intracaldera volcanism initiated at 197 BC and formed the present-day islands of Palaea and Nea Kameni. The magmatic vents of both lie within a NE-SW volcanotectonic line which control the magma ascent of the region and was reactivated (seismic epicenters) during the last volcanic unrest (2011-2012) (Parks et al., 2012). The evolution of the Kameni islands has been reported by 9 subaerial eruptions (Table 1) that discharged dacitic flows and formed domes, channels and levees, blocky lavas, ash plumes (Vulcanian eruptions) and ballistic ejecta (Fig. 36). Bathymetric imagery data have revealed submarine flows (pillow lavas) defining the actual morphology (pillow lavas) and final volume of products to 4.85±0.7 km^3 (Fig. 37) (Nomikou et al., 2014) instead of 4.3 ±0.7 km^3 (Fig. 38).

Table 1: Eruption historic records by previous authors (Fyticas et al., 1990; Druitt et al., 1999).

Eruption	Details
197 BC	Formation of Iera pyroclastic cone
46-47 AD	Extrusive activity and formation of Palaea Kameni
726 AD	Explosive activity on the northern part of Palaea Kameni
1570-3	NE vent migration – Mikra Kameni formation
1707-11	Effusive/explosive eruptions formed the NW part of Nea Kameni
1866-70	Effusive activity dominated the southern part of Nea Kameni
1925-28	NW explosive activity that united Nea with Mikri Kameni (Dafni crater)
1939-41	Phreatic eruptions - flows, domes of Ktenas, Fouque, Smith-Reck, Niki
1950	Extrusion of Liatsikas lavas (Center of Nea Kameni)

AD 46-47 (Palea Kameni). Appearance of a new island south-west of Hiera (at the location of the present day Palea Kameni), with a circumference of approx. 5600 m.

AD 726 (Palea Kameni). Explosive and effusive activity. The latter is responsible for lobe of blocky lava near Agios Nikolaos on the north-eastern side of Palea Kameni.

AD 1570 or 1573 (Mikra Kameni). Extrusion of a small lava dome - Mikri Kameni.

AD 1707-1711 (Nea Kameni). The first well-documented historical eruption of the Kameni islands. The eruption began in May 1707 with 'subterraneous fires, several violent earthquakes, a roaring noise, sulphurous exhalations and a black smoke' (Goree, 1707). Other reports include the formation of a white island to the west of Mikri Kameni which grew to ~ 70-80 m high and ~ 500-600 wide. Shortly after, a black island began to emerge and grow to the north of the white island. The black island and the white eventually merged in September 1707.

AD 1866-1870. (Nea Kameni). The largest historical eruption of the Kameni islands. The eruption commenced in late Jan/early Feb 1866. Fytikas et al., (1990) report that there were 'increases in seawater temperature, and some subsidence of the shores in Vulkano bay. The first lavas were slowly extruded, and the first explosions followed two days later.' At the beginning

Feb 1866 steam columns were observed and dark lava blocks rose to the surface of Vulkano bay. This site was named "Georgios". A second eruptive centre, called "Aphroessa" also formed to the south of Nea Kameni and in May 1866, 2 small islands appeared in the canal between Nea Kameni and Palea Kameni ("Maionisi", the May islands) but disappeared shortly thereafter.

AD 1925-1928 (Nea Kameni). Extrusion of lava domes (Daphne and Nautilus) and flows, summit crater explosions, and ash plumes. Growth of Nea Kameni to the north and east of the island filling the bay between Mikri Kameni and Nea Kameni. The start of the eruption (Aug 1925) was marked by vapour fountaining and a rise in sea temperature in the red bay (Kokkina Nera) on the eastern shore of Nea Kameni, combined with subsidence along the eastern coast and the extrusion of the Daphne lava dome. Explosive activity culminated in a phreatomagmatic column up to 3.3 km high. A pause in activity between May 1926 and Jan 1928 was followed by a series of phreatic explosions and the formation of the Nautilus lava dome.

Fig.36: Photos of Nea Kameni's historical eruptions.

AD 1939-1941 (Nea Kameni). Extrusion of lava domes (Triton, Ktenas, Fouqué, Smith-Reck and Niki) and flows, summit crater explosions and ash plumes. Phreatic explosions typically preceded episodes of lava extrusion. A rise in sea temperature in the bay of Agios Georgios, was observed ~ 3 months prior to the eruption.

AD 1950 (Nea Kameni). Extrusion of small lava dome (Liatsikas) preceded by phreatic explosions. The eruption lasted for less than one month.

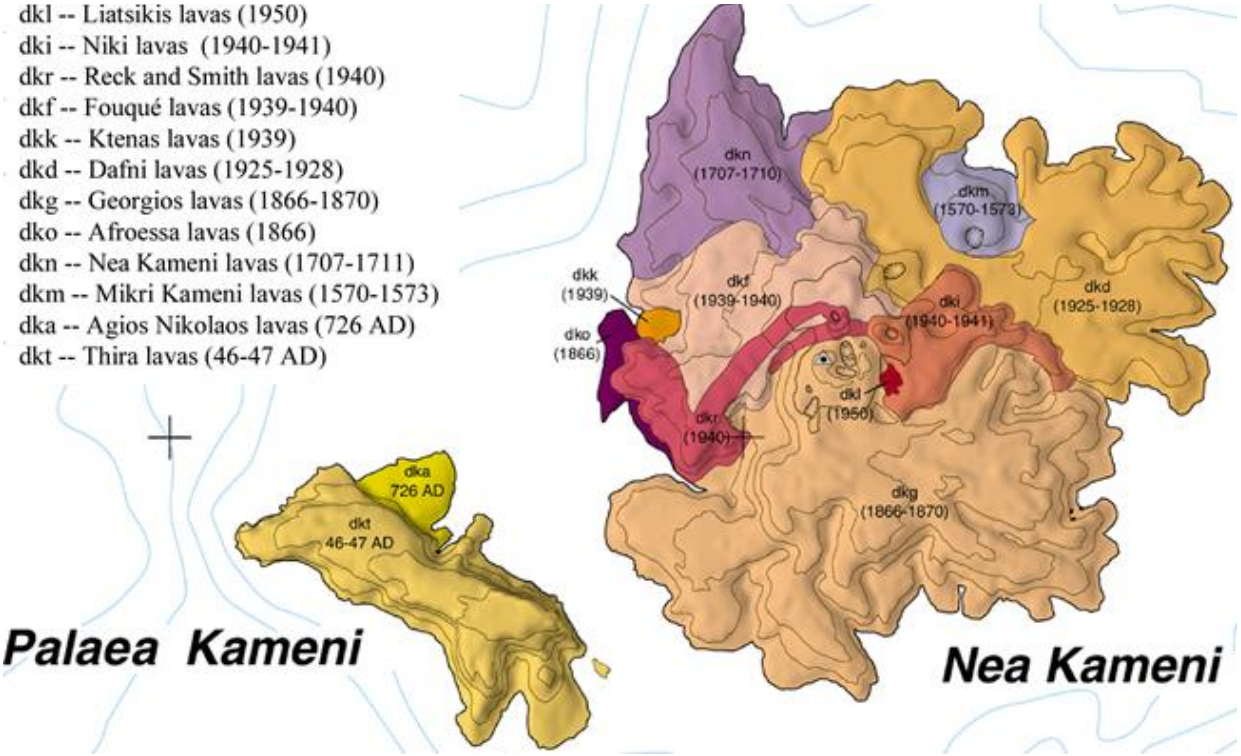

Fig.37: Geological map of the Kameni islands (Druitt et al., 1999).

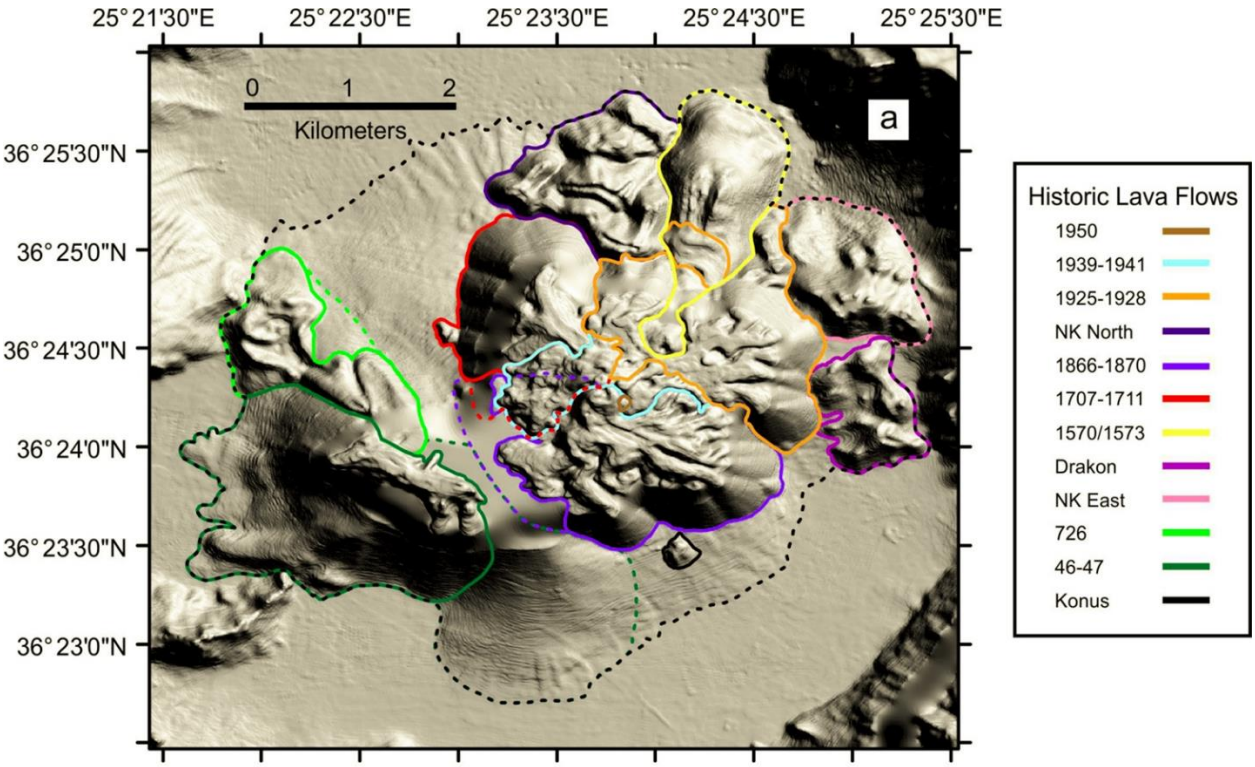

Fig.38: Onshore/offshore lava flow outlines for historic lava flows in the vicinity of the Kameni islands (Nomikou et al., 2014).

Features

The hiking path to the top (and central) part of the Nea Kameni volcano is permeating the last 3 eruptive periods of the post-minoan eruption flows. In general, during the first volcanic eruption period (1925-1928) volcanics were practically extruded in two phases forming the Dafni lavas which merged the Mikri Kameni island with the Nea Kameni edifice. The middle period (1939-1940) is divided into six distinct phases-flows which respectively formed the Ktenas, Fouqué, Smith (2 phases), Reck and Niki lavas (the WW2 lavas). The final effusive activity of the volcano, which occurred in 1950, formed the Liatsikas lavas. Besides the unrest period of 2011-2012 the volcano is still dormant.

The main volcanic products of the 3 last eruption periods were dacite domes and flows which created classic surface morphologies normally associated with viscous felsic lavas e.g. rafted blocks and blocky lavas, flow folds and layering, coulee and levee. In addition, gas escape and oxidation signs as well as different populations of magmatic enclaves have been observed and reported (Figs. 39, 40, 41).

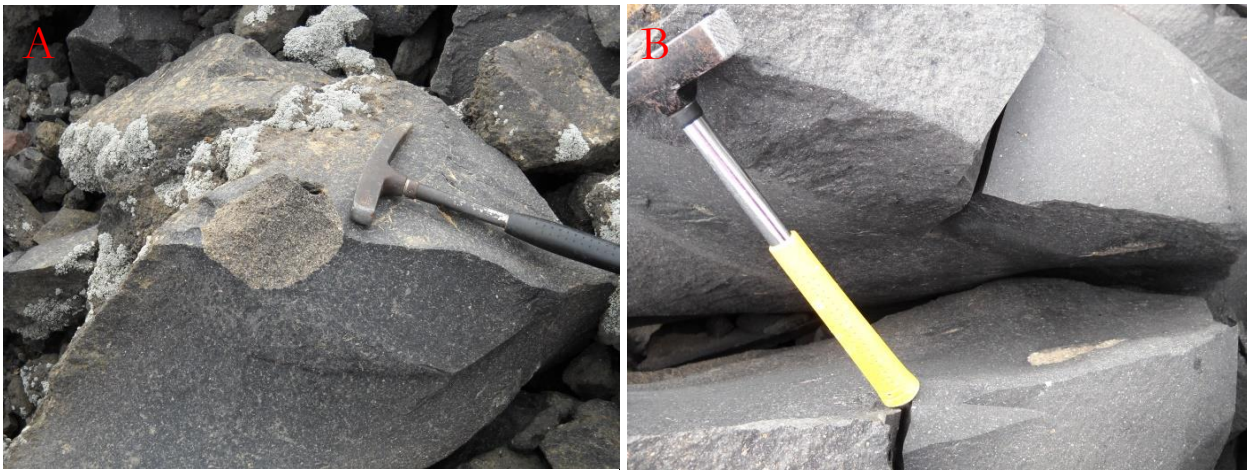

Fig.39: Magmatic enclaves observed at Dafni Lava flows (Drymoni et al., 2014).

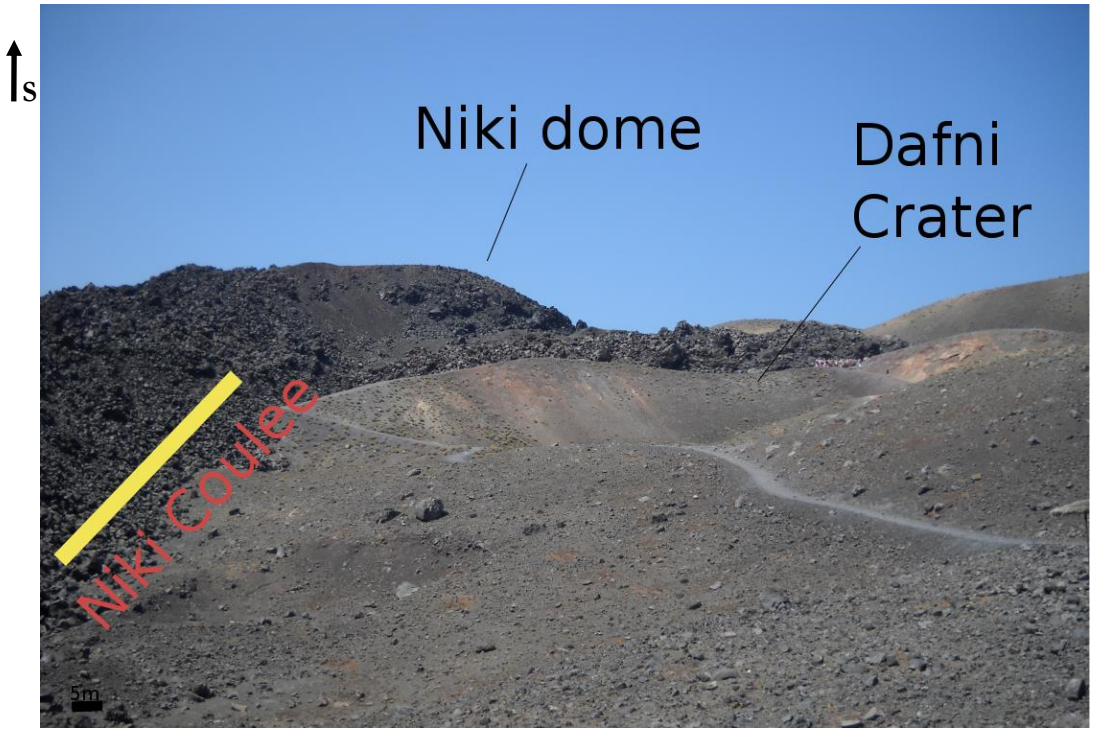

Fig.40: Coulee flow of Niki blocky lavas (1940-1941). At the front we observe the Dafni crater (1925), (Drymoni et al., 2014).

Fig.41: Layering and flow patterns (A), flow folds (B) observed at Liatsikas and Niki lava flows, (Drymoni et al., 2014).

Santorini Unrest 2011-2012

In January 2011, the caldera entered a phase of unrest that lasted until March of 2012. The number of small magnitude (M< 3.3) volcanotectonic earthquakes greatly increased at depths of 1-6 km on a near-vertical plane 6 km in length along the Kameni line (Newman et al., 2011) (Fig. 42). The increased seismicity was accompanied by up to about 10 cm inflation of the islands measured by GPS networks and by radar interferometry and corresponding to a volume increase of about 10-20 million m^3 at a depth of 3-6 km beneath the caldera (Newman et al., 2011; Parks et al., 2012; Papoutsis et al., 2012; Foumelis et al., 2013). Small increases in the flux of H_2 and of mantle-derived CO_2 also occurred during the unrest (Parks et al. 2013; Tassi et al. 2013).

The volume increase has been attributed to intrusion of magma (Newman et al. 2011; Parks et al 2012). The inflation may have involved fluids in addition to magma. It may also have been in part tectonic in origin, stress accumulation on regional faults (Feullet 2013) causing flexuring of the caldera block and increasing rock permeability and hence gas emissions (Tassi et al. 2013).

Parks et al. (2015) used a 20 year record of GPS and Insar data to reveal a slow (~6 mm/y) subsidence of southern Nea Kameni between 1993 and 2010, followed by unrest-related inflation of 2011-2012. The subsidence is attributed to thermal contraction and ground loading due to the 1866-70 lavas (Fig. 43). They modelled the unrest inflation as two intrusion pulses: one of 11.6 ± 0.1 million m^3, followed by another of 9.7 ± 0.1 million m^3, accompanied by a visco-elastic crustal response. The present repose period offers the opportunity for the scientific community, civil defence authority and local authorities to plan for a future eruption (Vougioukalakis et al., 2016).

Hooft et al., 2019 find a ~3-km-wide, cylindrical low-velocity anomaly in the upper 3 km beneath the north-central portion of the caldera, that lies directly above the pressure source of the 2011-2012 inflation. They interpret this anomaly as a low-density volume caused by excess porosities of between 4% and 28%, with pore spaces filled with hot seawater. Vents that were formed during the first three phases of the 3.6 ka Late Bronze Age (LBA) eruption are located

close to the edge of the imaged structure. The correlation between older volcanic vents and the low-velocity anomaly suggests that this feature may be long-lived. They infer that collapse of a limited area of the caldera floor resulted in a high-porosity, low-density cylindrical volume, which formed by either chaotic collapse along reverse faults, wholesale subsidence and infilling with tuffs and ignimbrites, phreatomagmatic fracturing, or a combination of these processes.

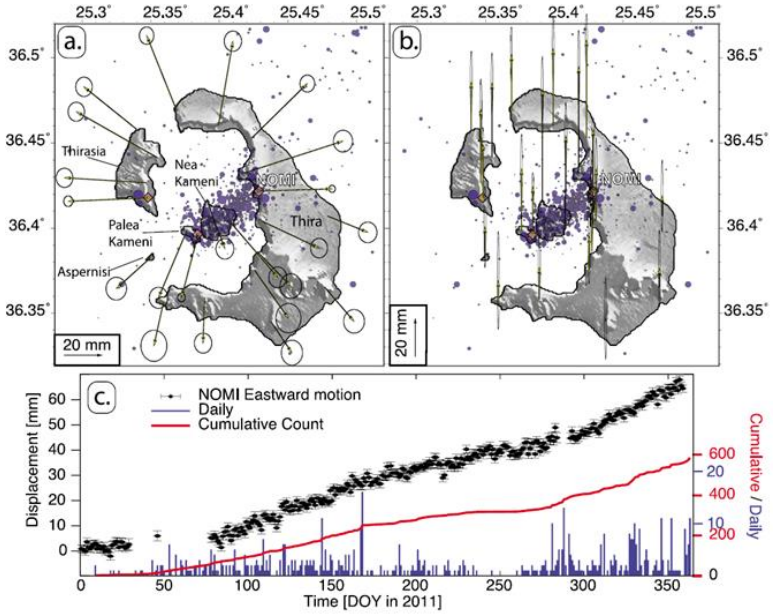

Fig.42: Unrest GPS data of Newman et al. (2012).

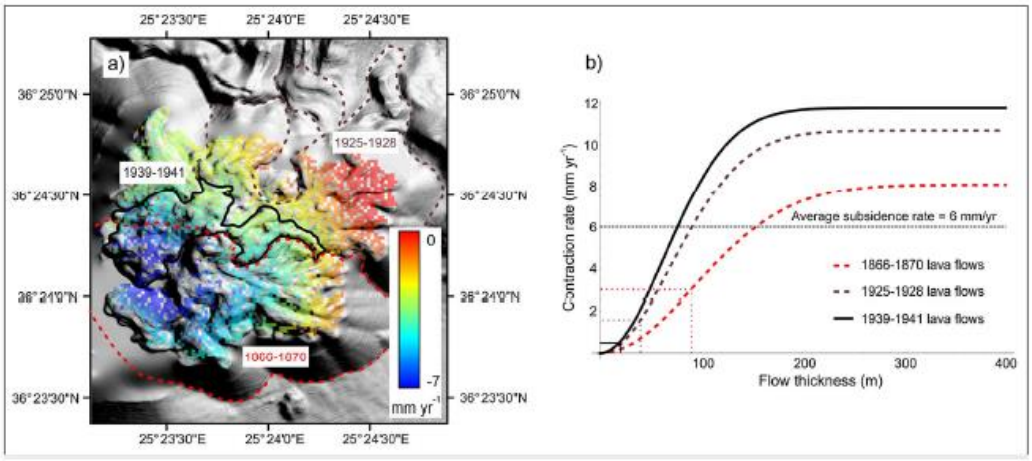

Fig.43: (a) Merged bathymetry and LiDAR grid after Nomikou et al. [2014], overlain with mean LOS displacements (mm/yr) computed using ascending Envisat interferograms from track 329. LOS displacement is negative away from the satellite. The red dashed polygon represents the outline of the 1866–1870 lava flow. The brown dashed polygon represents the outline of the 1925–1928 lava flow, and the black polygon represents the outline of the 1939–1941 lava flow. The dashed lines represent the extrapolated boundaries of the 1866–1870 and 1925–1928 lava flows. The northwest part of the 1866–1870 flow is thought to reside beneath the 1939–1941 lava flows. (b) Modeled thermal contraction rate of historic lava flows (mm/yr), plotted as a function of lava flow thickness (Parks et al., 2015).

The 1956 strong Amorgos Earthquake

Natural hazards from the Christiana–Santorini–Kolumbo (CSK) rift pose significant threats to the Eastern Mediterranean region, including earthquakes, subaerial or submarine volcanic eruptions, volcanic gas release, tsunamis due to eruptions or submarine landslides, and potential aviation problems from volcanic ash plumes (Nomikou et al., 2019). The great earthquake of Amorgos-Santorini with Magnitude 7.5 and a maximum perceived intensity of IX on the Mercalli intensity scale, occurred on July 9; 1956 and was the strongest event on the broader Aegean region during the 20th century followed by a tsunami (Fig. 44). The earthquake's focal mechanism is consistent with normal faulting, trending SW-NE. (Papadopoulos & Pavlides 1992; Okal et al., 2009). The earthquake, presumably caused by rapid extensional faulting, was accompanied by tsunamis with significant run-up along island coastlines (Nomikou et al. 2018).

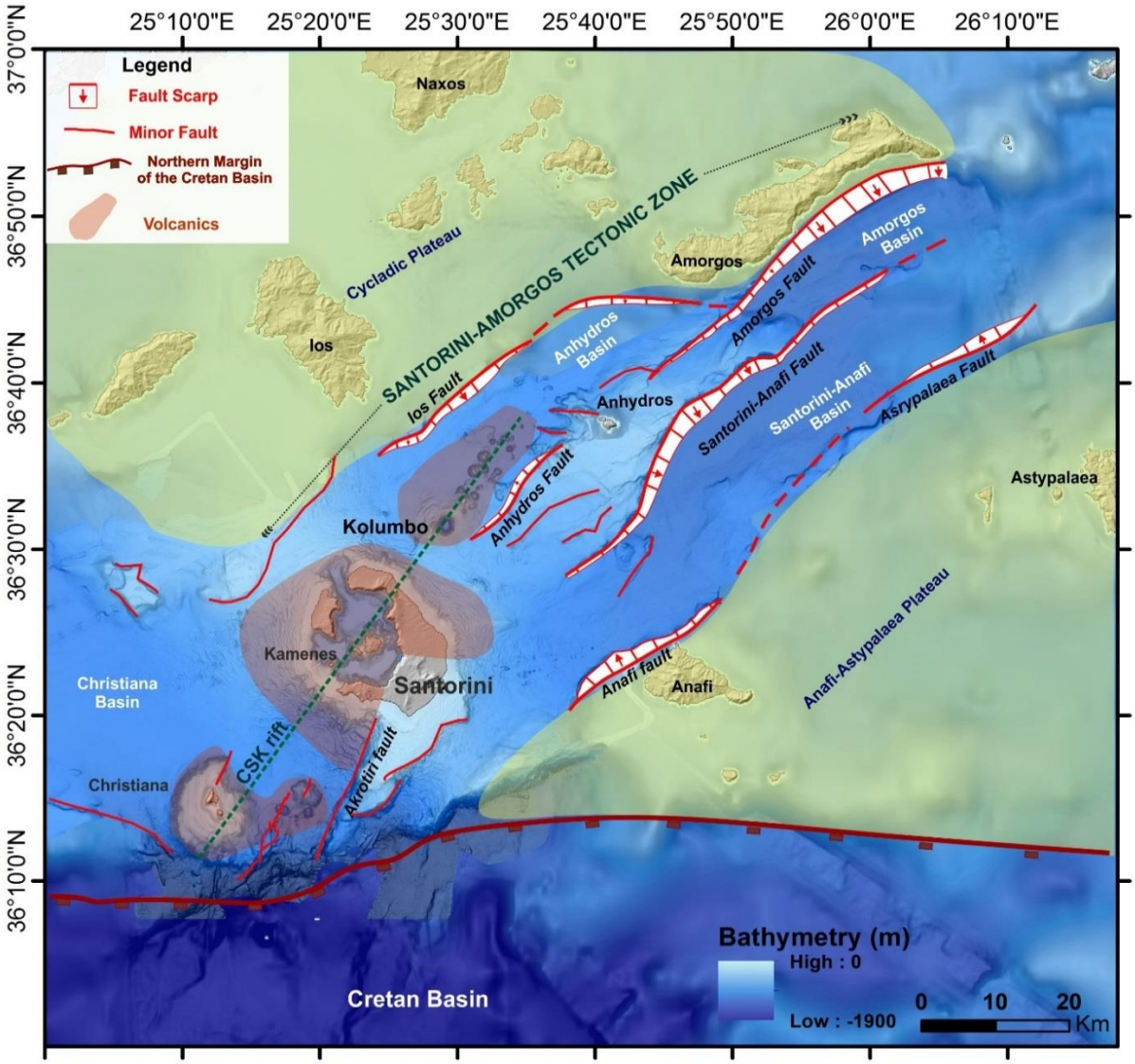

Fig.44: Major tectonic features of the Christiana–Santorini–Kolumbo (CSK) volcanic field and the Santorini–Amorgos Tectonic Zone (Nomikou et al., 2019).

COVER: Combined topographic map of Santorini Volcano based on onshore and offshore data (Nomikou et al. 2016).

INDEX MAP: Geological map of Santorini modified after (Druitt et al., 1999) showing the locations of the field-trip (stops).

REFERENCES

Anadón P., Canet C., Friedrich W. (2013). Aragonite stromatolitic buildups from Santorini (Aegean Sea, Greece): Geochemical and palaeontological constraints of the caldera palaeoenvironment prior to the Minoan eruption (ca 3600 yr bp). Sedimentology 60: 1128-1155

Antoniou, A. & Lekkas, E. (2010). 'Rockfall susceptibility map for Athinios port, Santorini Island, Greece', Geomorphology, vol. 118, pp. 152–166.

Antoniou V., Lappas S., Leoussis C. & Nomikou P. (2017). Landslide risk assessment of the Santorini volcanic group. GISTAM 2017 - Proceedings of the 3rd International Conference on Geographical Information Systems Theory, Applications and Management, pp.131.

Asku A. E., Jenner G., Hiscott R. N. and Isler E. B. (2008). Occurrence, stratigraphy and geochemistry of Late Quaternary tephra layers in the Aegean Sea and the Marmara Sea. Marine Geology, 252(3-4):174– 192.

Athanassas C.D., Bourlès D.L., Braucher R., Druitt T.H., Nomikou P., Léanni L. (2016). Evidence from cosmic ray exposure (CRE) dating for the existence of a pre-Minoan caldera on Santorini, Greece. Bulletin of Volcanology 78 (5).

Bond A. and Sparks. R.S.J. (1976). The Minoan eruption of Santorini, Greece Journal of the Geological Society of London 132: 1-16.

Browning J., Drymoni K., Gudmundsson A. (2015). Forecasting magma-chamber rupture at Santorini volcano, Greece. Sci. Rep. 5, 15785.

Bruins H. J., MacGillivray J. A., Synolakis C. E., Benjamini C., Keller J., Kisch H. J., Klügel A. and van der Plicht, J. (2008). Geoarchaeological tsunami deposits at Palaikastro (Crete) and the Late Minoan IA eruption of Santorini. Journal of Archaeological Science, 35(1):191–212.

Cadoux A., Scaillet B., Bekki S., Oppenheimer C., Druitt T.H. (2015). Stratospheric Ozone destruction by the Bronze-Age Minoan eruption (Santorini Volcano, Greece). Scientific Reports, 5, 12243.

Cioni R., Gurioli L., Sbrana A. and Vougioukalakis G. (2000). Precursory phenomena and destructive events related to the Late Bronze Age Minoan (Thera, Greece) and AD 79 (Vesuvius, Italy) Plinian eruptions; inferences from the stratigraphy in the archaeological areas. Geological Society of London Special Publication 171: 123-141.

Cita M.B. (1997). Geological and geophysical evidence for a Holocene tsunami deposit in the easternMediterranean deep-sea record, J. Geodyn., 24, 1–4.

Cita M. B. & Aloisi G. (2000). Deep-sea tsunami deposits triggered by the explosion of Santorini (3500 y BP) eastern Mediterranean. Shiki T., Cita, M. B. & Gorsline D. S. (Eds.), Sedimentary Features of Seismites, Seismo-turbidites and Tsunamites. Sedimentary Geology 135, 1–4, 181–203.

Doumas, C.G. (1983). Thera. Pompeii of the ancient Aegean. Thames and Hudson, London, 168pp.

Drymoni K., Magganas A., Pomonis P. (2014). Santorini Volcano's 20th Century Eruptions: A Combined Petrogenetical, Volcanological, Sociological and Environmental Study 2014EGUGA, 16.8405D.

Drymoni K. & Nomikou P. (2018). Field-Trip guide to Santorini Volcanic Complex. Staples Field Trip Seminar, Santorini 2018.

Druitt T. H. & Francaviglia V. (1992). Caldera formation on Santorini and the physiography of the islands in the late Bronze Age. Bull. Volcanol. 54, 484–493

Druitt T.H., Edwards L., Mellors R.M., Pyle D.M., Sparks R.S.J., Lanphere M., Davis M., Barriero B. (1999). Santorini Volcano. Geological Society Memoir No. 19, 165 p.

Druitt T.H. and Davies M.A. (1999). Geological map of the Santorini Islands, Aegean Sea, Greece. Scale 1:20,000. In: Druitt, T.H., Edwards, L., Davies, M., Lanphere, M.A., Mellors, R., Pyle, D., Sparks, R.S.J. and Barreiro, B (1999). Santorini Volcano. Memoir of the Geological Society of London 19, 176 pp.

Druitt T.H. (2014). New insights into the initiation and venting of the Bronze-Age eruption of Santorini (Greece), from component analysis. Bulletin of Volcanology 76, 794.

Druitt T.H., Francalanci L., Fabbro G. (2015). Field Guide to Santorini Volcano. MeMoVolc short course, Santorini, 2015.

Eriksen U., Friedrich W.L., Buchardt B., Tauber H., Thomsen M.S. (1990). The Stronghyle caldera: geological, palaeontological and stable isotope evidence from radiocarbon dated stromatolites from Santorini. In:

Hardy DA (ed.) Thera and the Aegean World III, vol 2. Thera Foundation, London, pp 139-150

Fabbro G., Druitt T.H., Scaillet S. (2013). Evolution of the crustal magma plumbing system during the build-up to the 22-ka caldera-forming eruption of Santorini (Greece). Bull Volcanol. 75:767.

Feuillet N. (2013). The 2011–2012 unrest at Santorini rift: stress interaction between active faulting and volcanism. Geophysical Research Letters 40, 3532-3537.

Foumelis M., Trasatti E., Papageorgiou E., Stramondo S. and Parcharidis I. (2013). Monitoring Santorini volcano (Greece) breathing from space. Geophysical Journal International, 193(1):161– 170.

Friedrich W.L. (2000) Fire in the Sea (translated by Alexander R McBirney). Cambridge University Press, Cambridge.

Friedrich W., Kromer B., Friedrich M., Heinemeier J., Pfeiffer T., Talamo S. (2006). Santorini eruption radiocarbon dated to 1627-1600 B.C. Science 312: 548.

Fytikas M., Kolios N., Vougioukalakis G. (1990). Post-Minoan volcanic activity of the Santorini volcano. Volcanic hazard and risk, forecasting possibilities. In: Hardy DA (ed.) Thera and the Aegean World III, vol 2. Thera Foundation, London pp 183-198.

Gudmundsson A. (2011). Rock fractures in geological processes. Cambridge University Press, Cambridge.

Heiken G. and McCoy F. (1984). Caldera development during the Minoan eruption, Thira, Cyclades, Greece. Journal of Geophysical Research, 89(B10):8441–8462.

Heiken G. and McCoy F.Jr. (1990). Precursory activity to the Minoan eruption, Thera, Greece. Thera and the Aegean World III (1990), Volume 2, Hardy D.A. (Ed.), The Thera Foundation, London, 79-88.

Hooft E.E.E., Nomikou P., Toomey D.R., Lampridou D., Getz C., Christopoulou M.-E., O'Hara, D., Arnoux G.M., Bodmer M., Gray M., Heath B.A., VanderBeek B.P., (2017). Backarc tectonism, volcanism, and mass wasting shape seafloor morphology in the Santorini-Christiana-Amorgos region of the Hellenic Volcanic Arc. Tectonophysics 712-713, pp.396.

Hooft E.E.E., Heath B.A., Toomey D.R., Paulatto M., Papazachos C.B., Nomikou P., Morgan J.V., Warner M.R. (2019). Seismic imaging of Santorini: Subsurface constraints on caldera collapse and present-day magma recharge. Earth and Planetary Science Letters 514, pp.48.

IGME (H.Pichler, D. Gunther, S. Kussmaul), (1980). Geological Map of Greece, Sheet Thera (1:50.000).

Johnston E. N., Sparks R. S. J., Phillips J. C. and Carey S. (2014). Revised estimates for the volume of the Late Bronze Age Minoan eruption , Santorini , Greece. Journal of the Geological Society of London, 171, 583–590.

Karátson D., Gertisser R., Telbisz T., Vereb V., Quidelleur X., Druitt T., Nomikou P., Kósik S. (2018). Towards reconstruction of the lost Late Bronze Age intra-caldera island of Santorini, Greece. Scientific Reports 8 (1).

Kelle, J., Ryan W. B. F., Ninkovich D. and Altherr R. (1978). Explosive volcanic activity in the Mediterranean over the past 200,000 yr as recorded in deep-sea sediments. Geological Society of America Bulletin, 89(4):591–604.

Keller J., Gertisser R., Reusser E. and Dietrich V. (2014). Pumice deposits of the Santorini Lower Pumice 2 eruption on Anafi island, Greece: Indications for a Plinian event of exceptional magnitude. Journal of Volcanology and Geothermal Research, 278-279.

Kilias A.A., D.M.. Mountrakis M.D. Tranos S.B. Pavlides S. (1998). The prevolcanic metamorphic rocks of Santorini Island: structural evolution and kinematics during the tertiary (South Aegean, Greece). Proceed. the 2nd workshop "The European Laboratory Volcanoes" Santorini, Greece 2-4 May 1996. European Commission. Volcanic risk. EUR 18161EN, 23-36.

Lister & Forster, (2007). Inside the Aegean Metamorphic Core Complexes, Edition Two, Reprinted from Journal of the Virtual Explorer, volume 27, paper 1.

Manning S.W., Ramsey C.B., Kutschera W., Higham T., Kromer B., Steier P., Wild E.M. (2006). Chronology for the Aegean Late Bronze Age 1700-1400 B.C. Science 312, 565–9.

Marinatos S. (1939). The volcanic destruction of Minoan Crete, Antiquity 13: 425-439.

Marinos V., Prountzopoulos G., Asteriou P., Papathanassiou G., Kaklis T., Pantazis G., Lambrou E., Grendas N., Karantanellis E., Pavlides S. (2017). Beyond the boundaries of feasible engineering geological solutions: stability considerations of the spectacular Red Beach cliffs on Santorini Island, Greece. Environ Earth Sci. 76:513.

McClelland E., Thomas R. (1990). A palaeomagnetic study of Minoan age tephra from Thera. In: Hardy DA (ed.) Thera and the Aegean World III, vol 2. Thera Foundation, London, pp 129-138.

Minoura K., Imamura F. and Kuran U. (2000). Discovery of Minoan tsunami deposits. Geology, 59–62.

Mountrakis D., Pavlides S., Chatzipetros A., Meletlidis S., Tranos M., Vougioukalakis G., Kilias A. (1998). Active deformation of Santorini, 2nd Workshop on "European Laboratory Volcanoes, Santorini, 2 - 4 May 1996, European Commission. Volcanic risk. EUR 18161EN Proceedings, 13 - 22.

Newman A.V., Stiros S., Feng L., Psimoulis P., Moschas F., Saltogianni V. and others (2012). Recent geodetic unrest at Santorini Caldera, Greece. Geophysical Research Letters 39 (L06309).

Nomikou P., Carey S., Papanikolaou D., Croff Bell K., Sakellariou D., Alexandri M., Bejelou K. (2012). Submarine Volcanoes of the Kolumbo volcanic zone NE of Santorini Caldera, Greece. Global and Planetary Change 90-91.

Nomikou, P., Papanikolaou, D., Alexandri, M., Sakellariou, D. and Rousakis, G. (2013). Submarine volcanoes along the Aegean volcanic arc. Tectonophysics, 597-598:123–146.

Nomikou P., Parks M., Papanikolaou D., Pyle D., Mather T., Carey S., Watts A., Paulatto M., Kalnins M., Livanos I., Bejelou K., Simou E., Perros I. (2014). The emergence and growth of a submarine volcano: The Kameni islands, Santorini (Greece). GeoResJ., Vol.1, 8-18.

Nomikou P., Druitt T.H., Hubscher C., Mather T.A., Paulatto M., Kalnins L.M., Kelfoun K., Papanikolaou D., Bejelou K., Lampridou D., Pyle D.M., Carey S., Watts A.B., Weib B., Parks M.M. (2016). Post-eruptive flooding of Santorini caldera and implications for tsunami generation. NATURE COMMUNICATIONS | 7:13332.

Nomikou P., Hübscher C., Papanikolaou D., Farangitakis P. G., Ruhnau M., Lampridou D. (2018). Expanding extension, subsidence and lateral segmentation within the Santorini - Amorgos basins during Quaternary: Implications for the 1956 Amorgos events, central - south Aegean Sea, Greece. Tectonophysics 722, pp.138.

Nomikou P., Hübscher C., Carey S. (2019). The Christiana–Santorini–Kolumbo Volcanic Field. Elements; 15 (3): 171–176.

Novikova T., Papadopoulos G. A. and McCoy F. W. (2011). Modelling of tsunami generated by the giant Late Bronze Age eruption of Thera, South Aegean Sea, Greece. Geophysical Journal International, 186(2), 665–680.

Oikonomidis D., Albanakis K., Pavlides S. and Fytikas M. (2016). Reconstruction of the paleo-coastline of Santorini Island (Greece), after the 1613 BC volcanic eruption: A GIS-based quantitative methodology. Journal of Earth System Science 125(1):1-11.

Paris R., Wassmer P., Lavigne F., Belousov A., Belousova M., Iskandarsyah Y., Benbakkar M., Ontowirjo B., Mazzoni N., (2014). Coupling eruption and tsunami records: the Krakatau 1883 case study, Indonesia. Bull Volcanol, 76:814.

Pavlides S., Chatzipetros A. (2018). The Fira fault (Santorini, Greece) from the French "Expédition de Morée (1829-38)" to modern scientific approach. Proc. 9th International INQUA Meeting on Paleoseismology, Active Tectonics and Archeoseismology, p. 218-220.

Okal E. A., Synolakis C. E., Uslu B., Kalligeris N. and Voukouvalas E. (2009). The 1956 earthquake and tsunami in Amorgos, Greece. Geophysical Journal International, 178(3):1533–1554.

Panagiotakopulu E., Higham T., Sarpaki A., Buckland P., Doumas C. (2013). Ancient pests: the season of the Santorini Minoan volcanic eruption and a date from insect chitin. Die Naturwissenschaften, 100 : 683– 689.

Papadopoulos, G. and S. Pavlides (1992). The large 1956 earthquake in the South Aegean: Macroseismic field configuration, faulting and Neotectonics of Amorgos Island. Earth Planet. Sc. Letters, 113, 383-396.

Papoutsis I., Papanikolaou X., Floyd M., Ji, K. H., Kontoes C., Paradissis D. and Zacharis V. (2012). Mapping inflation at Santorini volcano, Greece, using GPS and InSAR. Geophysical Research Letters, 40, 267–272.

Parks M.M., Biggs J., England, P., Mather T.A., Nomikou P., Palamartchouk K. and others (2012). Evolution of Santorini Volcano dominated by episodic and rapid fluxes of melt from depth. Nature Geoscience 5, 749–754.

Parks M.M., Moore J.D.P., Papanikolaou X., Biggs J., Mather T.A., Pyle D.M., Raptakis C., Paradissis D., Hooper A., Parsons B., Nomikou, P. (2015). From quiescence to unrest: 20 years of satellite geodetic measurements at Santorini volcano, Greece. Journal of Geophysical Research: Solid Earth, 120 (2), pp.1309.

Pfeiffer T (2001.) Vent development during the Minoan eruption (1640 BC) of Santorini, Greece, as suggested by ballistic blocks. Journal of Volcanology and Geothermal Research 106: 229-242.

Pyle D.M. (1990). New estimates for the volume of the Minoan eruption. In: Hardy DA (ed.) Thera and the Aegean World III, vol 2. Thera Foundation, London, pp 113-121.

Pyle D. (1997). The global impact of the Minoan eruption of Santorini, Greece. Environmental Geology 30: 59– 61.

Pyle, D.M. and Elliott, J.R. (2006). Quantitative morphology, recent evolution and future activity of the Kameni Islands volcano, Santorini, Greece. Geosphere 2, 253-268.

Rebesco M., Della Vedova B., Cernobori L. & Aloisi G. (2000). Acoustic facies of Holocene megaturbidites in the Eastern Mediterranean. Sedimentary Geology 135, 65–74.

Sigurdsson H., Carey S., Alexandri M., Vougioukalakis G., Croff K., Roman C., Sakellariou D., Anagnostou C., Rousakis G., Ioakim C., Gogou A., Ballas D., Misaridis T. and Nomikou P. (2006). Marine investigations of Greece's Santorini volcanic field. Eos, 87(34):337–348.

Simmons J.M., Cas R.A.F., Druitt T.H., Carey R.J. (2017). The initiation and development of a caldera-forming Plinian eruption (172 ka Lower Pumice 2 eruption, Santorini, Greece). J. Volcanol. Geotherm. Res. 341, 332–350.

Skarpelis N. and Liati A. (1990). The prevolcanic basement of Thera at Athinios: Metamorphism, Plutonism and Mineralization, Proc. of the Third International Congress "Thera and the Aegean World III", Hardy D.A. ed., The Thera Foundation, London, 2, 172- 182.

Sparks R.S.J., Wilson C.J.N. (1990). The Minoan deposits: a review of their characteristics and interpretation In: Hardy DA (ed.) Thera and the Aegean World III, vol 2. Thera Foundation, London, pp 89-99

Tassi F., Vaselli O., Papazachos C.B., Giannini L., Chiodini G., Vougioukalakis G.E., Karagianni E., Vamvakaris D. and Panagiotopoulos D. (2013). Geochemical and isotopic changes in the fumarolic and submerged gas discharges during the 2011–2012 unrest at Santorini caldera (Greece). Bulletin of Volcanology 75, 711.

Tema E., Kondopoulou D. and Pavlides S., (2013). Palaeotemperature estimation of the pyroclastic deposit covering the pre-Minoan palaeosol at Megalochori Quarry, Santorini (Greece): Evidence from magnetic measurements, Stud. Geophys. Geod., 57, 627-646.

Tema E., Zanella E., Pavón-Carrasco F.J., Kondopoulou D. and Pavlides S., (2015). Palaeomagnetic analysis on pottery as indicator of the pyroclastic flow deposits temperature: new data and statistical interpretation from the Minoan eruption of Santorini, Greece, Geophys. J. Int., 203, 33-47.

Vougioukalakis G., Sparks R.S.J., Pyle D., Druitt T., Barberi F., Papazachos C., Fytikas M. (2016). Volcanic hazard assessment at Santorini volcano: a review and a synthesis in the light of the 2011-2012 Santorini unrest. Bulletin of the Geological Society of Greece, vol. L, p. 274-283. Proceedings of the 14th International Congress, Thessaloniki, May 2016.

Watts A.B., Nomikou P., Moore J.D.P., Parks M.M., Alexandri M. (2015). Historical bathymetric charts and the evolution of Santorini submarine volcano, Greece. Geochemistry, Geophysics, Geosystems 16 (3), pp.847.